symmetry

MDPI

Article

Field-Theoretic Derivation of the Constructal Law from Non-Equilibrium Thermodynamics

Antonio F. Miguel [1,2]

[1] Department of Physics, School of Science and Technology, University of Evora, 7000-849 Evora, Portugal; afm@uevora.pt
[2] Complex Flow Systems Lab, Institute of Earth Sciences, Rua Romao Ramalho 59, 7000-671 Evora, Portugal

Abstract

Traditional analyses of transport phenomena rely on prescribed geometric boundaries, yet natural flow systems dynamically evolve their architecture to maximize access to currents. To address this disparity, we propose a field-theoretic framework for the constructal law that treats physical geometry as a dynamic state variable, represented by a time-dependent conductivity tensor. Using a variational approach grounded in non-equilibrium thermodynamics, we derive a general tensor evolution equation. Within this framework, macroscopic flow architecture emerges deterministically from the continuous competition between nonlinear flux-induced accretion, linear entropic relaxation, and spatial smoothing. Scaling analysis reduces this dynamic to a tri-parameter dimensionless phase space: a morphogenic number driving structural growth, a structural diffusion number governing spatial coherence, and a stochastic intensity number providing the microscopic seeds for symmetry breaking. Our principal result is the analytical prediction of a critical bifurcation. When the local morphogenic number strictly exceeds unity, the system escapes its stable, isotropic configuration and branches into highly conductive, anisotropic architectures. We demonstrate the predictive validity and trans-scalar applicability of this continuum theory by mapping it to highly diverse phase transitions, successfully capturing phenomena ranging from microscopic aerosol agglomeration and microbial resistance, to macroscopic coral plasticity and crystal growth instabilities, and finally to the astrophysical launching of relativistic jets from black holes.

Keywords: non-equilibrium thermodynamics; morphological phase transition; tensor field theory; constructal law; symmetry breaking; Mullins–Sekerka instability

Academic Editors: Sergei Odintsov and Calogero Vetro

Received: 12 March 2026
Revised: 21 April 2026
Accepted: 23 April 2026
Published: 24 April 2026

1. Introduction

The classical formulation of transport phenomena relies fundamentally on the assumption of prescribed geometric boundaries. Within this paradigm, the spatial configuration of a system (whether mediating thermal, mechanical, or electromagnetic fields) serves as a static boundary condition, providing the immutable manifold over which conservation laws are integrated to resolve the state variables. This perspective has now reversed. The focus is not only on the dynamics of fluxes within a control volume, but on the thermodynamic evolution of the geometry itself, where flow actively structures the domain to extremize global access. This shift from assuming geometry to deriving it represents a fundamental development in science [1]. In engineering, this shift is manifest in the move from parametric sizing to generative design and topology optimization. Here, material distributions co-evolve with principal axes to guide vector fields toward optimal configurations [2].

In non-equilibrium thermodynamics, this appears in the study of spontaneous pattern formation, where systems break symmetry to extremize their rate of entropy production [3,4]. Under this framework, a system configuration is elevated from a mere boundary condition to a primary, dynamic physical property whose evolution governs global performance and persistence.

The realization that macroscopic physical properties are determined not merely by intrinsic chemistry, but by the precise geometric arrangement of matter, suggests a fundamental equivalence between structure and function. While this principle is engineered in metamaterials to synthesize effective constitutive parameters (e.g., permittivity and permeability) from sub-wavelength unit cells [5,6], and is classically demonstrated in living systems through the compatibility between a cell's compartmental structure and its biological function, it manifests most profoundly as a macroscopic dynamic process in non-equilibrium systems. This concept extends into continuum mechanics through topology optimization, which treats the material distribution not as a fixed boundary, but as a variable field that evolves to extremize a physical objective [2,7,8]. Remarkably, this optimization is not limited to computational algorithms. Natural systems exhibit an analogous, spontaneous morphological adaptation. Under the influence of thermodynamic stress, flow architectures across all scales break symmetry to distribute resistive losses and maximize transport efficiency. Bejan and co-authors [1,9–11] frame this evolutionary imperative as the so-called constructal principle which states "For a finite size flow system (not infinitesimal) to persist in time (to live) it must evolve with freedom such that it provides easier and greater access to what flows". This imperative is observable across disparate physical scales, where geometry adapts dynamically to imposed fluxes. In geophysics, river basins self-organize into fractal networks to maximize the drainage of water flux from area to point [12]. In biophysics, vascular systems evolve hierarchical branching architectures to minimize the hydrodynamic dissipation required to perfuse tissue [1,13]. In electrodynamics and plasma physics, dielectric breakdown patterns (lightning) branch stochastically to maximize the rate of charge neutralization through a resistive medium [14]. According to this framework, the physics of design generation is fundamentally a morphing process, where the system evolves its architecture to distribute resistances and minimize the global dissipation of flow. Collectively, this diverse body of literature, spanning metamaterial engineering, geophysical self-organization, and biological allometry, demonstrates that the spontaneous emergence of flow architecture is not a collection of isolated anomalies, but a universal thermodynamic imperative. However, this literature predominantly treat the final evolved architectures as static geometric optimizations or rely on separate, discipline-specific phenomenological rules. What remains notably absent from the literature is a cohesive, generalized mathematical formulation capable of deterministically deriving this structural evolution across all these scales.

This transition from identifying the tendency of configuration to predicting the trajectory of configuration requires an evolution in the theoretical framework itself. Although the constructal principle provides the powerful physical intuition that flow systems evolve to extremize access, its operationalization as a predictive tool demands a rigorous mathematical formalism. It successfully identifies the macroscale direction of evolution, yet a governing field equation is required to determine the local, continuous path of that evolution. The history of physics illustrates that the maturity of a theoretical framework is often marked by the distillation of physical insight into a canonical field equation [14–16]. Just as early geometric intuitions regarding electromagnetism and gravity were eventually codified into the rigorous field equations of Maxwell [15] and Einstein [16], the phenomenological observation of flow architecture now requires its own formal governing equation.

To address this gap, the explicit aim of this study is to propose a mathematical framework that conceptualizes flow architecture not as a static geometric boundary condition, but as a dynamic, anisotropic tensor field evolving under the imperative of thermodynamic stress. Unlike a scalar or vector representation, a second-rank tensor is mathematically mandatory here because it alone can fully encode the broken spatial symmetries, principal axes of flow, and orthogonal resistances inherent to an evolved transport network. The novelty of this approach lies in integrating the constructal imperative with Ginzburg–Landau phase-field modelling. This synthesis contributes new insight by establishing the evolution of design as a formal boundary-value problem in non-equilibrium field theory, allowing for the deterministic calculation of morphological bifurcations rather than relying on heuristic optimization.

To substantiate the trans-scalar application of this deterministic approach, we also explicitly apply the governing evolution equation to five distinct physical regimes: the microscopic agglomeration of aerosols, the mesoscopic growth of stony corals, crystal growth, the evolutionary expansion of microbial colonies, and the morphological phase transitions of astrophysical accretion disks and relativistic jets.

2. Field-Theoretic Formulation for the Dynamic Evolution of Flow Architectures

A comprehensive description of far-from-equilibrium transport phenomena, applicable across scales, necessitates a mathematical framework that reconceptualizes flow architecture, not as a static geometric optimum, but as a continuous field evolving under thermodynamic stress. This formalism promotes the domain configuration to a dynamical degree of freedom, co-evolving with the currents it supports on a generalized n-dimensional manifold Ω. Rather than a loose analogy, we employ a phenomenological Ginzburg–Landau framework [17] where the principles of non-equilibrium thermodynamics serve as strict mathematical isomorphisms for gradient-driven transport. Specifically, the mathematical derivation of this framework rests on three foundational physical assumptions: (i) the system is strictly gradient-driven, (ii) the structural matrix behaves as a yielding medium capable of dynamic spatiotemporal reconfiguration, and (iii) the generalized free energy of the configuration can be expanded following the lowest-order permitted tensor symmetries. As detailed in the Appendix A, the step-by-step derivation procedure follows a strict thermodynamic sequence. First, a scalar functional is constructed from the invariants of the local flux and conductivity tensors. Second, Hohenberg–Halperin relaxational dynamics (Model A) are applied to calculate the deterministic downhill descent of the energy landscape via Euler–Lagrange functional derivatives. Finally, to ensure physical objectivity in moving media, the resulting local descent is upgraded using an objective material tensor rate, and stochastic fluctuations are introduced to permit symmetry breaking.

2.1. Formulation of the State Fields

To ensure this description satisfies the criteria of determinism and closure, the system is fully characterized by the interaction of three fundamental fields. The generalized flux density $J(x, t)$ is required to enforce local conservation laws (continuity equations). This vector field quantifies the transport of extensive quantities (mass, charge, or momentum), ensuring that the time evolution of the system adheres to the conservation of mass and energy. In addition, the scalar potential $\phi(x, t)$ is required to satisfy the second law of thermodynamics. This field represents the intensive driving force (e.g., pressure, temperature, or voltage), where $-\nabla\phi$ defines the thermodynamic gradient that impels the flux, ensuring the flow proceeds in the direction of entropy production. To close the system dynamically, the configuration field $K(x, t)$ is required. While classical kinematics treats material prop-

erties as fixed background constraints, we introduce K as a time-dependent conductive tensor (encoding local conductivity, permeability, or geometry). Importantly, this tensorial format allows the geometry to represent both perfectly uniform isotropic states and highly directional anisotropic architectures. To clarify the distinction between this framework and classical kinematics, the 'geometry' of the flow system is defined here not as a set of prescribed, immobile boundaries, but as a field-theoretic manifestation of the conductivity tensor K(x, t). In this framework, the global shape and architectural boundaries of the system are emergent properties (mathematically represented as the spatial integrals of local tensor states) rather than static constraints provided a priori. By treating the configuration as a continuous state variable, the 'boundaries' of the flow paths correspond to the moving interfaces where the local conductivity transitions from the isotropic background to highly anisotropic, conductive pathways. This allows the system to escape the limitations of fixed-grid geometry, deriving the global manifold as a deterministic solution to the local variational evolution.

Its evolution is governed by the variation in the action with respect to the local flow intensity, thereby rendering the configuration of the system a deterministic outcome of field interactions rather than an arbitrary boundary condition. In this framework, the emergence of macroscopic shape and morphological bifurcations is derived from first principles as the coupled solution to these three field equations.

The instantaneous interaction between these fields is governed by the necessity to satisfy local conservation laws and the second law of thermodynamics. We postulate a phenomenological ansatz for the generalized constitutive transport relation, which links the thermodynamic force to the resulting flux

$$J = -\mathrm{K}(x, t, \|\nabla\phi\|).\nabla\phi, \tag{1}$$

Here K acts as the generalized conductivity tensor, mapping the potential gradient to the flux. While this form encompasses linear regimes (such as Darcy flow or Ohm's law, where K is independent of the driving force), it extends to non-linear transport phenomena. In complex regimes, such as turbulent flow, or high-field drift, deviations from linearity are absorbed into the dependence of the tensor K on the field invariants (e.g., shear rate or gradient magnitude). Notice that K is defined as a symmetric second-rank tensor. This tensorial rank is physically mandatory because the emergence of flow architecture is synonymous with symmetry breaking. An evolved system must possess intrinsic directionality (anisotropy), facilitating flux along principal axes while presenting resistance orthogonal to them. The thermodynamic driver for this evolution is the local dissipation density σ. It is mathematically and physically mandatory to stress that while the conductivity and fluxes are tensorial and vectorial, the rate of entropy production σ is a scalar quantity. It is defined by the contraction of the flux with the conjugate driving force

$$\sigma = J.(-\nabla\phi) \geq 0, \tag{2}$$

Substituting the constitutive relation (Equation (1)) into this definition yields the quadratic form $\sigma = \nabla\phi.K.\nabla\phi$. Consequently, to strictly satisfy the second law of thermodynamics ($\sigma \geq 0$) for all possible field configurations, the mobility tensor $\mathrm{K}(x, t, \|\nabla\phi\|)$ must be positive definite. Thus, Equation (2) identifies the specific sites of maximal entropy production. In our framework, these sites act as the active zones for morphological adaptation, where the system is most stressed to restructure itself. Depending on the evolutionary imperative, this restructuring will either facilitate transport (e.g., growing highly conductive dendritic networks to maximize access) or actively minimize transport

(e.g., precipitating insulating layers or impermeable biological barriers to shield against harmful fluxes).

2.2. The Evolution Equation

While Equations (1) and (2) characterize the instantaneous thermodynamic state of the flow, the core of the approach lies in the temporal dynamics of the manifold itself. To determine the temporal evolution of the conductivity tensor, we employ a formal variational approach based on non-equilibrium thermodynamics, specifically utilizing the Hohenberg–Halperin Model A relaxational dynamics derived in the Appendix A. According to Equation (A7) in the Appendix A, the time-evolution of the conductivity tensor is governed by the superposition of four competing physical tendencies (positive feedback, entropic relaxation, spatial regularization, and stochastic fluctuations) expressed as an objective tensor rate equation

$$\tau \overset{o}{K} = \alpha(J \otimes J) - \beta \mathrm{K} + \gamma \nabla^2 K + \xi(x,t), \tag{3}$$

Here, τ represents the characteristic relaxation time of the structural medium, defining the temporal scale of the morphological response relative to the convective flow dynamics. The coefficients α, β, γ and ξ are not arbitrary fitting parameters but fundamental physical constants determined by the constitutive properties of the domain. Specifically, α quantifies the accretion efficiency or material susceptibility to flux-induced stress, β defines the volumetric rate of entropic decay or structural maintenance cost, γ represents the intrinsic spatial stiffness or structural diffusion of the medium, and ξ scales the variance of random environmental or thermal fluctuations.

To explicitly demonstrate the self-referential nature of the structural evolution, we substitute the constitutive relation (Equation (1)) into the accretion term of Equation (3). This yields a closed-form evolution equation for the conductivity tensor

$$\tau \overset{o}{K} = \alpha[(\mathrm{K}.\nabla\phi) \otimes (\mathrm{K}.\nabla\phi)] - \beta \mathrm{K} + \gamma \nabla^2 K + \xi(x,t), \tag{4}$$

The application of this framework is governed by the physical nature of the medium. In strictly rigid media with predefined geometries (e.g., laminar flow constrained within a rigid cylindrical pipeline, or standard heat conduction in a solid block), the structural relaxation time approaches infinity ($\tau \longrightarrow \infty$). Consequently, the material cannot physically yield to the thermodynamic stress, forcing the evolution of the conductivity tensor to vanish ($\mathrm{K} \longrightarrow 0$). At this limit, the tensor K(x, t) ceases to be a dynamic degree of freedom and freezes into a static spatial boundary condition K(x). The non-linear morphogenic feedback loop completely decouples, and the proposed framework mathematically collapses back into the classical formulation of transport phenomena, where the flux J is simply resolved over an immutable geometric manifold. However, in yielding or morphing media (such as granular beds, soft biological tissues, or astrophysical plasmas), τ is finite, and the material matrix dynamically reconfigures under transport stress. Thus, this equation reveals the fundamental non-linearity of the morphogenic process. The source term scales quadratically with the local conductivity tensor dependence (because the dyadic product $[(\mathrm{K}.\nabla\phi) \otimes (\mathrm{K}.\nabla\phi)]$ results in $\mathrm{O}(\mathrm{K}^2)$), creating a positive feedback loop where regions of higher conductivity attract greater flux, which in turn drives further growth in conductivity.

Significantly, the dyadic structure $[(\mathrm{K}.\nabla\phi) \otimes (\mathrm{K}.\nabla\phi)]$ governs the dual role of symmetry in this framework. Mathematically, the configuration tensor K must remain strictly symmetric to obey the Onsager reciprocal relations of non-equilibrium thermodynamics, preventing the emergence of non-physical rotational fluxes. Because the dyadic product of any vector with itself inherently produces a perfectly symmetric tensor, the structural

accretion term naturally preserves the mathematical symmetry of the K manifold. However, morphologically, this term drives the absence of spatial symmetry. It ensures that structural growth is not isotropic, but is strictly aligned with the principal axis of the thermodynamic gradient, forcing the material to break spatial symmetry and evolve into an anisotropic, highly directed transport architecture. However, this tensor evolution cannot operate in isolation. Because the non-linear structural accretion requires a continuous driving flux, the canonical evolution equation must be coupled with a secondary transport, continuity, or diffusion-reaction equation governing the local scalar potential (ϕ). As the evolving structural manifold (K) dynamically facilitates mass flow, consumes nutrients, or dissipates latent heat, this secondary equation must continuously recalculate the available potential field. Mathematically, this is formalized by enforcing local conservation of the relevant extensive quantity via a generalized continuity equation. By equating the divergence of the flux to any local source or sink terms S(x, t), and substituting the constitutive relation (Equation (1)), we obtain the governing elliptic equation $\nabla.(\mathrm{K}\nabla\phi) = -S(x,t)$. Solved continuously over the domain Ω, this equation dynamically recalculates the scalar potential field as the structural conductivity K yields. Once the new potential field is established, the constitutive relation (Equation (1)) is utilized to map the thermodynamic gradient to the dynamically updated flux J. This updated flux is then fed back into the tensor evolution equation for the subsequent time step, establishing a continuous mathematical coupling between the thermodynamic transport of the medium and the geometric evolution of the domain.

While Equations (3) and (4) describe this coupled local rearrangement of material, strictly local growth could lead to unbounded conductivity. To represent a physical system with finite resources (e.g., a fixed volume or a limited construction budget), we impose a global constraint on the trace of the tensor (the total amount of conductive material)

$$\int_{\Omega} Tr(K(x,t))d^n x = C_0, \tag{5}$$

Here, the operator Tr(·) denotes the trace of the tensor. Physically, the sum of the principal conductivities is proportional to the local porosity or mass density of the transport network. Therefore, integrating this trace over the domain yields the constant C_0, representing the fixed global resource pool (e.g., total available biological mass, fluid volume, or construction material), ensuring that the growth of structure is a zero-sum redistribution rather than unbounded generation. This global integral constraint is enforced during the temporal evolution of Equation (3) by treating the dissipation coefficient β as a dynamic Lagrange multiplier. By continuously adjusting β at each time step, the system guarantees that local structural accretion is perfectly balanced by non-local relaxation, thereby preserving the constant resource pool C_0 and making the morphological evolution a strict zero-sum redistribution. While this global coupling renders the true late-stage evolution non-local, the onset of morphological instability operates on a much faster timescale than global resource depletion. Thus, the initial symmetry-breaking bifurcations are governed by the local linear stability of the tensor field under a quasi-static constitutive baseline for β. While β acts as a dynamically adjusting variable to strictly conserve mass during transient growth phases, analyzing the fundamental stability and phase transitions of the system requires evaluating it near equilibrium. Therefore, for the following scaling analysis, we treat β as the steady-state, macroscopic dissipation rate ($\beta \approx \beta_0$) required to maintain the global resource pool C_0 against entropic decay.

2.3. Dimensionless Scaling

We perform next a scaling analysis to decouple the fundamental physics from arbitrary dimensional constraints. By introducing characteristic scales for the macroscopic domain size L, the potential driving force ϕ_0, and a reference conductivity K_0 imposed by the global resource constraint, we define a set of dimensionless variables $x^* = x/L$, $K^* = K/K_0$ and $\phi^* = \phi/\phi_0$. The term ξ^* represents the normalized stochastic field, which accounts for random structural noise or thermal fluctuations within the medium, and is defined by dividing the raw stochastic field $\xi(x, t)$ by its characteristic intensity σ_ξ that represents the stochastic intensity scale (i.e., it quantifies the variance of the random fluctuations affecting the conductivity tensor K). Furthermore, we define the characteristic time scale of the structural evolution as $\tau^* = \tau/\beta$, representing the natural relaxation lifetime of a fluctuation in the absence of forcing, such that $t^* = t/\tau^*$. To scale the material derivative, we define a dimensionless velocity vector u^* as the ratio between the local material velocity field u (which commands the convective transport of the medium) and the characteristic velocity scale U, where the characteristic velocity scale is defined strictly by the intrinsic kinematics $U = L\beta/\tau$, yielding the dimensionless objective rate operator $\overset{o}{K}$.

Substituting these variables into Equations (3) and (4) and normalizing by the linear damping scale βK_0, we obtain the canonical dimensionless evolution equation

$$\overset{o}{K^*} = \Pi_1(J^* \otimes J^*) - K^* + \Pi_2 \nabla^{*2} K^* + \Pi_3 \xi^*, \tag{6}$$

$$\overset{o}{K^*} = \Pi_1[(K^*.\nabla^*\phi^*) \otimes (K^*.\nabla^*\phi^*)] - K^* + \Pi_2 \nabla^{*2} K^* + \Pi_3 \xi^*, \tag{7}$$

with

$$\Pi_1 = \frac{\alpha K_0 \phi_0^2}{\beta L^2} \qquad \Pi_2 = \frac{\gamma}{\beta L^2} \qquad \Pi_3 = \frac{\sigma_\xi}{\beta K_0}, \tag{8}$$

where Π_1 is a morphogenic number, Π_2 is a structural diffusion number, and Π_3 is a stochastic intensity number.

Notice that this transformation reveals that the phase space of the system is fundamentally spanned by these two dimensionless groups (the morphogenic number Π_1 and the structural diffusion number Π_2), which act as the primary control parameters determining the morphogenic regime. The morphogenic number represents the ratio of flow-induced ordering forces to entropic decay forces, and quantifies the gain of the positive feedback loop. It serves as the critical order parameter for the system, and crucially, acts as a direct mathematical measure of the system's distance from global thermodynamic equilibrium. As the system is driven far from equilibrium by intense external forcing, it crosses the critical threshold ($\Pi_1 > 1$), where non-linear accretion mathematically overwhelms the damping. Conversely, if the system remains near equilibrium ($0 < \Pi_1 < 1$), linear decay dominates, and the system maintains a heavily damped, mildly isotropic geometry. This framework also naturally answers the theoretical limit of what occurs in the absolute absence of thermodynamic flow. If the flux vanishes ($J \longrightarrow 0$, yielding $\Pi_1 = 0$), the non-linear accretion term disappears entirely. The structural evolution becomes strictly governed by entropic decay ($-\beta K$) and spatial smoothing ($\gamma \nabla^2 K$). Thermodynamically, because maintaining an ordered, anisotropic architecture requires continuous energy input, a flowless system must melt or relax. The geometry is reduced to a completely homogeneous, isotropic, and featureless background state, representing absolute diffusive equilibrium where the material is uniformly distributed according to the global resource constraint C_0. Conversely, if $\Pi_1 < 1$ but non-zero, the linear decay dominates, but the system maintains a heavily damped, mildly isotropic geometry. However, performing a linear stability analysis on Equation (6) reveals that if $\Pi_1 > 1$, the non-linear accretion mathematically

overwhelms the damping ($\Pi_1(J^* \otimes J^*) > \mathrm{K}^*$). At this critical bifurcation point, the system to spontaneously break symmetry and bifurcate into stable, anisotropic transport states. Physically, this instability corresponds to the spontaneous localization of global flux into discrete, high-performance pathways aligned with the driving gradient.

The structural diffusion number Π_2 represents the ratio of structural smoothing forces to entropic decay forces. This value defines the intrinsic correlation length of the architecture relative to the system size and controls the characteristic wavenumber of the spatial perturbation modes. A small Π_2 admits high-frequency spatial modes, facilitating the formation of complex, fine-grained structures. For example, in vascular systems, this regime corresponds to fractal-like capillary beds. A large Π_2 suppresses small-scale fluctuations, forcing the system to evolve into globally coherent, low-frequency structures, physically analogous to broad, smooth conduits.

The stochastic intensity number Π_3 represents the ratio of random structural fluctuations to the deterministic relaxation rate. This parameter governs the robustness of the emerging architecture against microscopic or environmental noise. The impact of this noise evolves distinctly across the stability timeline. Before bifurcation (in the sub-critical regime, $\Pi_1 < 1$), the noise induces only transient, heavily damped ripples in the conductivity field. At the exact threshold of instability, it acts as the critical nucleation mechanism, providing the microscopic perturbations required to break spatial symmetry. After bifurcation (in the super-critical regime, $\Pi_1 > 1$), the noise determines the specific spatial selection (e.g., the exact direction a dendrite branches) before its influence is largely overpowered by the deterministic, non-linear growth of the primary structures. If Π_3 is sufficiently large, it may disrupt the global coherence of the transport network, leading to a fragmented or noisy morphology where the deterministic ordering of Π_1 is partially suppressed by stochasticity.

In summary, this highlights a core dualism within the framework, the interplay between deterministic thermodynamic evolution and stochastic exploration. The deterministic groups (Π_1 and Π_2) dictate the potential energy landscape of the system, defining the strict energetic thresholds where a new configuration becomes thermodynamically favorable or unstable. However, determinism alone cannot break a perfectly symmetric, isotropic state. The stochastic intensity (Π_3) acts as the essential causal agent (the physical explorer) that continuously probes this deterministic landscape. It is the stochastic noise that discovers the unstable pathways and provides the microscopic seeds necessary to trigger symmetry breaking. Consequently, this dualism transforms the emergence of flow architecture from a purely deterministic, preordained descent into a dynamic process of exploration and settlement, where the system harvests its own internal noise to escape local minima and actualize the deterministic imperative.

To conceptualize this morphological phase space, one can envision a generalized stability diagram spanned by these two dimensionless parameters. As will be explicitly demonstrated in the system-specific applications later in this work, the condition $\Pi_1 = 1$ serves as the general separatrix delineating the isotropic and anisotropic regimes. Simultaneously, the magnitude of Π_2 acts as an orthogonal axis determining structural complexity, tuning the evolved architecture along a spectrum from highly ramified, fractal-like networks (low Π_2) to thick, singular conduits (high Π_2). Finally, Π_3 provides a third dimension of variability, defining the threshold of structural stability and the degree of randomness inherent in the final evolved form.

The derivation presented in this section yields a fundamental theoretical conclusion. The emergence of complex flow architectures is not the result of a global optimization algorithm, but rather the deterministic, local spatiotemporal equilibrium of non-equilibrium matter. By reducing the physical phase space to the interaction of the morphogenic drive (Π_1), spatial cohesion (Π_2), and stochastic exploration (Π_3), this formulation establishes

that symmetry breaking and morphological adaptation are inevitable thermodynamic requirements for any yielding medium subjected to a critical flux gradient.

3. Field-Theoretic Formulation of the Constructal Law

The operationalization of the constructal law requires a precise mapping from its original thermodynamic statement [1,9–11]:

> *"For a finite size flow system (not infinitesimal) to persist in time (to live) it must evolve with freedom such that it provides easier and greater access to what flows"*

into the formalism of non-equilibrium field theory. This mapping necessitates redefining the system state not through static geometric parameters, but through three interacting continuum fields:

(i) The objective function is quantified by the generalized current density vector J (representing the flow to be facilitated);
(ii) The driving potential is defined by the gradient $\nabla\phi$ (representing the thermodynamic stress);
(iii) The configuration is represented by the time-dependent conductivity tensor field K.

In this framework, the geometry of the flow architecture is no longer an independent boundary condition but a dynamical state variable. The "finite size" requirement of the law is explicitly operationalized by the global integral constraint (Equation (5)), which ensures the system is not an idealized infinitesimal point but a macroscopic domain with a fixed resource budget C_0. This enforces a non-local competition where the "greater access" achieved in one sub-domain necessitates the concomitant relaxation of underutilized regions, making evolution a zero-sum redistribution of transport capacity.

The temporal evolution of this configuration is governed by Equation (3), the mathematical embodiment of the constructal law.

The imperative to provide "easier and greater access" is implemented by the non-linear accretion term, $\alpha(J \otimes J)$. Here, "access" is a strictly quantifiable thermodynamic objective: the maximization of the local flux vector J for a given potential gradient. Similarly, the resulting "flow architecture" corresponds to the emergent anisotropic principal axes of the conductivity field K. As flux magnitude J increases, the local conductivity grows and aligns its principal eigenvalues with the flow direction, representing a directional optimization to facilitate greater throughput along the path of highest stress. Furthermore, the "evolution with freedom" is represented by the coupling of the objective material rate $\overset{o}{K}$ and the stochastic intensity Π_3. The objective rate ensures the architecture is free to rotate and move with the medium, while Π_3 provides the "causal agent" that allows the system to escape unstable configurations and discover organized architectures that maximize efficiency.

To demonstrate cross-disciplinary scope, we map these dynamics into a dimensionless phase space. The morphogenic number Π_1 acts as the threshold for seeking "easier access"; when $\Pi_1 > 1$, the drive to facilitate flow overwhelms entropic decay, forcing morphogenesis. The structural diffusion number Π_2 determines the morphological fineness of that access, while the stochastic intensity Π_3 governs structural stability and provides the perturbations required to trigger symmetry breaking. Together, these parameters uniquely map the evolution of the dimensionless conductivity as it responds to the normalized flux tensor.

We can thus articulate a canonical, field-theoretic definition of the constructal law:

> *"The conductivity field of any driven system spontaneously breaks symmetry to maximize flow access. This macroscopic architecture emerges as a dissipative structure, where the non-linear drive of the flow overpowers entropic decay, ignited by microscopic noise"*

This reformulation offers three critical theoretical advantages that solidify the framework's physical and mathematical foundation. First, it ensures mathematical consistency

and objectivity by employing the material derivative, which allows the configuration field to be preserved along material trajectories rather than being restrained to a static coordinate frame. By utilizing the dyadic product $\alpha(J \otimes J)$, the model further derives the emergence of anisotropy from first principles without the need for ad hoc geometric assumptions. Second, the framework establishes strict causality through the Langevin approach, demonstrating that order arises from bottom-up local interactions rather than top-down mandates. In this context, the system utilizes intrinsic fluctuations to explore the energy landscape, effectively transforming structural evolution from a purely deterministic descent into a dynamic process of exploration and settlement where the "flux-coupling torque" drives the final architecture. Finally, and perhaps most significantly, this approach transforms the principle of global resistance minimization from an axiomatic postulate into a derived theorem. The system is shown to asymptotically approach a state of maximal access not because it possesses a goal-oriented "seek" function, but as a necessary mathematical consequence of the underlying dynamics governed by the dimensionless groups Π_1, Π_2, and Π_3. Collectively, these advantages ground the constructal law in the fundamental principles of non-equilibrium field theory, providing a robust, predictive mechanism for the self-organization of flow architectures.

4. Application Across Scales

To substantiate the cross-disciplinary scope of the proposed field approach, we next apply the governing formalism defined by Equations (3)–(8) to the morphological evolution of flow architectures across five distinct physical regimes. In each regime, we examine whether the system adheres to the definition of the constructal principle established herein, investigating if the emergent configuration arises as the deterministic result of the competition between flux-induced conductivity enhancement and dissipative structural decay.

To evaluate these phase transitions, the continuous field equations derived in Section 2 can be solved numerically. The general research approach for the simulated systems follows a step-by-step computational procedure: (i) the domain is initialized with a uniform or stochastically seeded isotropic conductivity tensor (K); (ii) a secondary diffusion-reaction or heat equation is numerically solved across the domain to establish the scalar potential field (ϕ) and the available macroscopic gradients; (iii) the local thermodynamic flux (J) is calculated using the constitutive relation (Equation (1)); (iv) this updated flux is fed into the canonical tensor evolution equation (Equation (3)), which calculates the local spatial accretion, dissipation, and smoothing; and (v) the structural manifold is updated for the subsequent time step. These numerical simulations were executed using custom Python 3.14 scripts, utilizing finite-difference spatial discretization to accurately capture the Laplacian smoothing operators and the non-linear dyadic tensor interactions. By holding the mathematical solvers constant and only altering the dimensionless parameters (Π_1, Π_2, Π_3) according to the specific physical regime, we isolate the universal thermodynamic mechanics driving the morphological evolution.

To formalize the mathematical equivalence across these disparate regimes before detailing them individually, Table 1 explicitly maps the generalized theoretical parameters of our governing tensor evolution (Equation (3)) to their domain-specific physical counterparts. This demonstrates how the universal abstract mechanics of accretion, dissipation, and spatial smoothing are instantiated across fundamentally different physical laws.

Table 1. Phenomenological mapping of field-theoretic parameters across physical scales.

Physical Regime	Scalar Potential ϕ	Generalized Flux J	Accretion/Drive α	Dissipation/Decay β	Spatial Smoothing γ	Stochastic Seeds ξ
Aerosol agglomeration	Electric potential	Dielectrophoretic mass flux	Electrostatic dipole accretion	Volumetric entropic decay	Surface tension/compactness	Random particle deposition
Stony corals	Nutrient concentration	Nutrient flux	Metabolic calcification rate	Maintenance/starvation tax	Hydrodynamic tissue cohesion	Localized polyp irregularities
Crystal growth	Temperature/solute field	Latent heat/solute flux	Latent heat/supercooling drive	Interfacial attachment kinetics	Gibbs–Thomson capillarity	Microscopic thermal fluctuations
Microbial resistance	Chemoattractant gradient	Chemotactic biomass flux	Mutational supply $\times$ velocity	Antibiotic toxicity/mortality	Bacterial random motility	De novo mutational noise
Relativistic jets	Gravitational/Metric potential	Energy-momentum flux	Magnetic Maxwell stress	Radiative cooling penalty	Viscous spreading/coherence	MHD turbulence variance

4.1. Microscopic Agglomeration Dynamics

We first apply our formalism to the aggregation of aerosol particles under electrostatic fields [18]. The morphological evolution is governed by the competition between the electrostatic accretion of mass, the geometric diffusion of the accumulation, and the stochastic noise inherent in particle-by-particle deposition. In this regime, the system trajectory is defined by the interaction of the morphogenic number Π_1, the structural diffusion number Π_2, and the stochastic intensity Π_3. While the former two parameters determine the energetic viability and permissible characteristic spatial perturbation modes, the noise scaled by Π_3 represents the fundamental structural fluctuations, random clusters of aerosol deposition, that probe the stability of the evolving manifold.

Mapping the general variables to this physical context, the structuring coefficient α represents the electrostatic accretion efficiency. Here, the general thermodynamic variables map directly to electrostatics. The scalar potential ϕ is the electric potential (voltage V), and the generalized flux J is the mass flux of particles driven by the dielectrophoretic force. Unlike the generic case, the effective drive in this scenario is intrinsically scale-dependent. As the characteristic dimension D of the spherical aggregate grows, the mean charge-dipole attractive force exerted on the surrounding aerosols decays geometrically. Because this electrostatic pull is dynamically balanced by the viscous Stokes drag of the ambient fluid, the convective deposition velocity, and consequently the radial mass flux intensity, diminishes proportionally to the inverse square root of the aggregate diameter ($|J| \propto D^{-1/2}$) [18]. Consequently, the canonical definition of the morphogenic number is renormalized to reflect this screening, yielding an effective electrostatic drive Π_1 that scales inversely with the system size

$$\Pi_1 = \frac{\alpha |J|^2}{\beta K} \propto \frac{\alpha V^2}{\beta D}, \tag{9}$$

In this constitutive definition, each parameter plays a distinct thermodynamic role. The α acts as the phenomenological coupling constant quantifying the susceptibility of the medium to dipole-field accretion, V represents the fixed intensive potential difference driving the transport, β denotes the linear dissipation coefficient, representing the thermodynamic cost per unit volume to maintain structural order against entropic decay, and D serves as the evolving screening length scale that modulates the effective field intensity.

This scaling reveals a critical thermodynamic bottleneck. In the initial morphogenesis phase ($t \longrightarrow 0$), where D is small relative to the external field curvature, the effective drive is high, yet the topology is dominated by the smoothing term $\gamma \nabla^2 K$. The diffusion term imposes a penalty on sharp gradients, effectively acting as a surface tension that minimizes the surface-to-volume ratio. Mathematically, this Laplacian operator suppresses high-wavenumber spatial modes, forcing the conductivity tensor K to evolve isotropically. Thus, the system relaxes into a compact, spherical morphology, representing a stable, isotropic solution where the entropic maintenance cost ($-\beta K$) is balanced by the uniform radial accretion. However, as the aggregate expands isotropically, it induces a shielding

effect on its own nutrient supply, driving the system toward a saturation fixed point where the structural dissipation $-\beta K$ (which is extensive and scales with volume) begins to overwhelm the dwindling accretion source term Π_1/D. The spherical morphology thus becomes thermodynamically self-limiting. Furthermore, the topological evolution is strictly governed by the structural diffusion number, Π_2, which scales inversely with the square of the aggregate dimension. In the initial morphogenesis phase, when D is small, Π_2 is exceedingly large. This high structural diffusion number dominates the phase space, strictly enforcing the isotropic spherical morphology by suppressing high-wavenumber surface perturbations. However, as the aggregate expands continuously, the system is driven into a low-Π_2 regime. When this rapid drop in spatial regularization intersects with the thermodynamic bottleneck defined by Π_1, the system transitions to a complex geometry. This transition is not an artifact of purely deterministic drift but is actively mediated by the stochastic intensity Π_3. In the initial high-Π_3 regime, random structural perturbations are immediately damped by the dominant spatial regularization. However, as the aggregate expands and Π_2 collapses, the system becomes very sensitive to the noise floor defined by Π_3. At this critical juncture, these previously negligible fluctuations are no longer suppressed. Instead, they serve as the essential seeds that trigger the transition from the isotropic spherical state to a differentiated configuration. The transition to a complex geometry is therefore not a random fluctuation, but a deterministic stability requirement imposed by Equation (3) when the system dimension D exceeds a critical wavelength for stability

$$\lambda_c \sim \sqrt{\frac{\gamma}{\alpha |J|^2}}, \tag{10}$$

At this bifurcation point, the isotropic solution becomes unstable to high-wavenumber surface perturbations. A nascent perturbation on the surface, stochastically promoted by Π_3, triggers local flux enhancement. In this unstable regime, the local flux J_{tip} decouples from the macroscopic screening length D and becomes determined solely by the local curvature. This localization creates a massive spike in the accretion term $\alpha(J_{tip} \otimes J_{tip})$, which locally overwhelms the global damping β and the smoothing penalty γ. The dyadic nature of this source term introduces a non-linear positive feedback loop. Increased local curvature enhances the flux J, which quadratically amplifies the structural growth rate, driving the system away from the linear equilibrium. Consequently, the system breaks symmetry, abandoning the spherical mode for a collimated dendritic architecture. This needle mode is the energetically favored state because its entropy production formally exceeds that of the spherical mode, allowing the system to penetrate the screening envelope and access a linear growth regime despite the global resource constraints. In the context of granular aggregation, this theoretical prediction is confirmed by the experimentally observed transition at $D_{crit} \sim 6\ r_p$ [18], where r_p is the particle radius, which corresponds to the geometric stability limit ($\sim 2\pi\ r_p$) where the system circumference naturally accommodates a fundamental perturbation matching the particle scale.

4.2. Morphological Transitions in Biological Growth

We next examine the morphological transition in stony corals, which exhibit phenotypic plasticity, shifting from compact hemispherical mounds in high-advection environments to complex branching dendrites in low-advection environments [19–21]. The morphological evolution of the colony is described by evolution Equation (3), driven by the interplay between hydrodynamic transport constraints and the internal competition between non-linear metabolic accretion (α), entropic decay (β), and spatial smoothing (γ).

To map this biological transition, we must evaluate the system across two distinct spatial scales: the macroscopic diffusion boundary layer L_{disp} dictated by hydrodynamics,

and the intrinsic structural length scale of the biological tissue (e.g., the polyp radius), r_0. This competition is fully parameterized by the simultaneous evolution of the morphogenic number (Π_1), the structural diffusion number (Π_2), and the stochastic intensity (Π_3). While Π_1 and Π_2 define the metabolic viability and the permissible characteristic spatial perturbation modes, the noise scaled by Π_3 represents the fundamental structural fluctuations, random irregularities in calcification or polyp distribution, that probe the stability of the evolving colony surface.

In environments characterized by high advection (high Reynolds number, Re >> 1), strong external currents continuously replenish the nutrient field. The boundary layer is compressed such that $L_{disp} \approx r_0$. Because the nutrient supply is forcibly uniform, the isotropic flux across the colony surface is governed strictly by the intrinsic scale $J_{iso} \approx K_0 \phi_{bulk}/r_0$. Normalizing Equation (3) with this intrinsic length scale yields a globally robust morphogenic number

$$\Pi_1 = \frac{\alpha K_0 \phi_{bulk}^2}{\beta r_0^2}, \Pi_2 = \frac{\gamma}{\beta r_0^2}, \tag{11}$$

In this high-advection regime $\Pi_1 > 1$, the non-linear accretion term globally overwhelms the metabolic decay term $-\beta K$. Because the system is metabolically satiated everywhere, there is no thermodynamic stress driving symmetry breaking. Furthermore, the thin boundary layer drives an extremely high Π_2. This massive structural diffusion mathematically ensures that the topological evolution is dominated by the smoothing term $\gamma \nabla^2 K$, which acts as an energetic surface tension. It suppresses any localized high-wavenumber perturbations, forcing the system to naturally relax into a stable, compact, and perfectly symmetric hemispherical mound. In low-advection environments (Re $\longrightarrow$ 0), transport becomes heavily limited by molecular diffusion, resulting in the formation of a thick depletion boundary layer $L_{disp} >> r_0$. As this depletion zone expands, the macroscopic gradient $\nabla \phi$ diminishes. The global isotropic flux drops significantly to $J_{iso} \approx K_0 \phi_{bulk}/L_{disp}$. This hydrodynamic state alters the thermodynamic stability of the entire system. The macroscopic morphogenic number drops strictly below the viability threshold

$$\Pi_{1,mac} = \frac{\alpha K_0 \phi_{bulk}^2}{\beta L_{disp}^2} < 1, \Pi_{2,mac} = \frac{\gamma}{\beta L_{disp}^2} << 1, \tag{12}$$

This condition indicates that the isotropic mound solution has become metabolically untenable. The volumetric decay term $-\beta K$ now overwhelms the dwindling accretion term. The spherical mound is effectively dying. The simultaneous collapse of Π_2 means the system no longer possesses the structural stiffness required to enforce spatial uniformity. The energetic penalty for creating new surface interfaces vanishes, suddenly permitting the high-wavenumber spatial modes required for dendritic branches to form. At this precise threshold, the transition is catalyzed by the stochastic intensity Π_3. In high-advection environments, any surface irregularity is immediately suppressed by the dominant spatial regularization of Π_2. However, as the advection drops and $\Pi_{2,mac}$ collapses, the system becomes very sensitive to the noise floor defined by Π_3. These previously negligible fluctuations are no longer smoothed away. Instead, they serve as the essential microscopic seeds that probe the stagnant boundary layer, seeking the nutrient-rich field beyond the depletion zone. To survive this starvation constraint, the system must undergo a morphological phase transition (symmetry breaking) to access a path of lesser resistance.

This is mechanically realized through diffusive flux focusing. Because $\Pi_{2,mac}$ is now functionally negligible, a stochastic perturbation or nascent bump emerging from the surface, promoted by the intensity Π_3, is no longer smoothed away. With a radius of curvature r_0, it penetrates the stagnant boundary layer. The local gradient at the tip of this

protrusion is no longer governed by the macroscopic layer L_{disp}, but by spherical diffusion at its own tip, restoring the local flux to $J_{iso} \approx K_0\, \phi_{bulk}/r_0$. This creates a massive geometric divergence in the tensor evolution equation. At the valleys of the perturbation, the system is screened (L_{disp} dominates, $\Pi_1 < 1$, tissue decays or stalls). At the tip, the constructal drive is restored to its intrinsic maximum ($\Pi_{1.local} >> 1$).

$$\tau \frac{\partial K_{tip}}{\partial t} >> \tau \frac{\partial K_{valley}}{\partial t}, \tag{13}$$

Because the source term $\alpha(J \otimes J)$ scales quadratically with this local flux, the tip experiences a runaway non-linear feedback loop. The spatial disparity between the dying valleys and the thriving tip mathematically forces the elongation of the bump into a stable branch. Thus, the transition from mound to dendrite is not triggered by an increase in global resources, but by the collapse of $\Pi_{1,mac}$ and $\Pi_{2,mac}$. Branching is the deterministic, mathematical escape mechanism, a localized symmetry breaking triggered by stochastic seeds and permitted by a lack of spatial regularization ($\Pi_2 \longrightarrow 0$) that allows the system to sustain $\Pi_{1,local} > 1$ in a globally starved field.

4.3. Morphological Transitions in Crystal Growth

We next examine the morphological transition in crystal growth, where solid–liquid interfaces dynamically restructure under thermal and solutal gradients. According to the formulation in Section 2, the geometry of the flow architecture is not a static boundary but a dynamical state variable governed by the continuous tensor field evolution. To validate this continuum approach, we map its abstract dimensionless phase space directly to the foundational morphological stability limits of binary alloys presented by Sekerka [22].

The transition from a stable, isotropic seed to a highly branched dendrite is determined by the continuous competition between flux-induced accretion, entropic decay, and spatial smoothing. In the context of alloy solidification, the generalized state fields mapped in Section 2.1 take on specific physical identities. The scalar potential ϕ represents the combined thermodynamic field of temperature and solute concentration, while the generalized flux J describes the convective flow of latent heat and rejected solute away from the moving interface. The mathematical mechanics of the tensor evolution equation (Equation (3)) translate clearly into the variables of the Mullins–Sekerka instability [23,24]. The non-linear accretion term ($\alpha(J \otimes J)$) mirrors the constitutionally driven concentration gradient that actively destabilizes the interface. The linear entropic decay term ($-\beta K$) represents the stabilizing thermal gradient acting across the solid and liquid phases, as well as the inherent drag of interfacial attachment kinetics. Finally, the spatial smoothing term ($\gamma \nabla^2 K$) is the direct field-theoretic equivalent of the Gibbs–Thomson capillarity effect, which imposes a strict energetic penalty on sharp interfacial curvature.

By normalizing these competing forces, the system is fully parameterized by the morphogenic number (Π_1) and the structural diffusion number (Π_2), which together describe the complex stability boundaries mapped in Figure 11 of Sekerka's [22] analysis. The morphogenic number mathematically represents the ratio of the destabilizing solutal drive to the stabilizing thermal decay. At low growth velocities, the spatial regularization enforced by Π_2 is massive relative to the convective flux. In this regime, the system operates below the critical bifurcation threshold ($\Pi_1 < 1$). The linear decay overwhelms the accretion drive, and the powerful spatial smoothing forces the crystal to maintain a diffusion-limited, perfectly symmetric isotropic shape, such as a smooth sphere or planar front. This deterministic behavior corresponds precisely to the stable region bounded by the modified constitutional supercooling criterion on the low-velocity left side of Sekerka's Figure 11 [22].

As the growth velocity increases or the ambient concentration is elevated, the flux of latent heat and rejected solute rises quadratically. This surge drives the morphogenic number strictly above unity ($\Pi_1 > 1$), indicating that the local thermodynamic drive to facilitate flow has overwhelmed the linear decay. Concurrently, the experimentally observed drop in tip radius indicates that the spatial regularization dictated by Π_2 collapses relative to the overwhelming accretion drive. When this drop in capillarity-driven smoothing intersects with the high solutal drive, the microscopic thermal fluctuations (parameterized in the field theory by the stochastic intensity number (Π_3)) are no longer suppressed. These Π_3 fluctuations serve as the essential microscopic seeds that trigger localized symmetry breaking. The system crosses the boundary into the interior of the U-shaped curve in Sekerka's Figure 11 [22], entering the unstable dendritic regime. Here, a runaway positive feedback loop is initiated: microscopic protrusions penetrate the boundary layer, steepen the local flux gradient J, and morph deterministically into highly conductive primary dendritic arms. Ultimately, it is this inherent stochasticity that makes every crystal unique. When the growing system enters a highly energetic, unstable state, unsuppressed microscopic thermal fluctuations act as random seeds that trigger localized symmetry breaking. These probabilistic shifts dictate exactly where runaway protrusions will pierce the boundary layer before deterministically morphing into uniquely branched dendritic arms.

The predictive consistency of this mapped formulation is revealed at extreme growth velocities, perfectly mirroring the absolute stability limit defined by Sekerka [22]. As velocity continues to increase toward the absolute stability threshold, the critical wavelength for instability (plotted in Figure 10 of Sekerka's study [22]) diverges toward infinity because the destabilizing effect of the solute is completely negated by capillarity. In the language of our tensor formulation, the macroscopic length scales compress so severely at extreme velocities that the structural diffusion number (Π_2) rebounds, effectively neutralizing the non-linear morphogenic drive (Π_1) at the microscopic level. Consequently, the effective local drive drops back below unity. The system crosses back over the right-hand boundary of the U-shaped curve in Sekerka's Figure 11 [22], escaping the dendritic phase and deterministically restabilizing into an isotropic, planar geometry.

To visualize this continuous thermodynamic trajectory, Figure 1 maps the structural evolution of the conductivity tensor directly across the theoretical boundaries established by Sekerka [22]. Figure 1 illustrates a unified stability phase diagram spanned by the growth velocity and the concentration drive, overlaid with the canonical U–shaped separatrix that delineates the $\Pi_1 = 1$ bifurcation threshold. Embedded within this phase space are sequential spatial snapshots of the tensor field K at three distinct time-steps of an accelerating growth trajectory. In Step A (low velocity), the system resides outside the left boundary of the U–curve; $\Pi_1 < 1$ and high Π_2 force the tensor field into a compact, isotropic seed. In Step B (intermediate velocity), the trajectory breaches the separatrix, entering the interior of the U–curve where $\Pi_1 > 1$, amplified Π_3 fluctuations break symmetry, and the density field violently branches into a complex dendritic architecture to maximize flux access. Finally, in Step C (extreme velocity), the trajectory exits the right side of the U-curve. Absolute capillary stability suppresses the structural diffusion modes, returning the system to a smooth, restabilized isotropic front. Thus, the complex sequence of crystal morphologies is proven to be a deterministic trajectory through the dimensionless phase space defined by the tensor evolution equation.

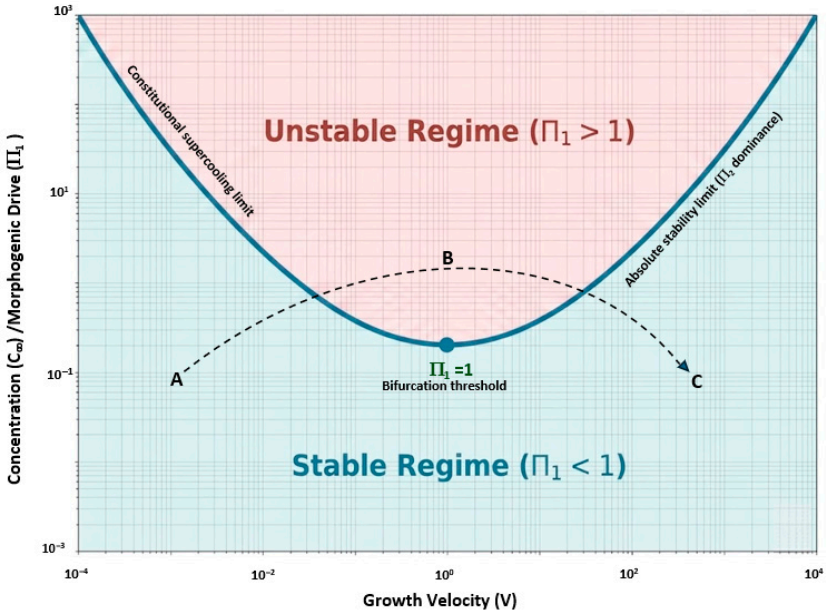

Figure 1. Constructal stability phase diagram mapping the field-theoretic evolution of the conductivity tensor K to the classical Mullins–Sekerka instability in crystal growth. The U–shaped separatrix rigorously delineates the critical bifurcation threshold ($\Pi_1 = 1$). While the *y*-axis scales with the morphogenic drive ($\Pi_1 \propto C_\infty$), the *x*-axis (V) inversely controls the structural diffusion number (Π_2). In the stable regime ($\Pi_1 < 1$), strong spatial smoothing enforces an isotropic configuration, bounded by the constitutional supercooling limit at low velocities (Step A) and absolute capillary stability (Π_2 dominance) at extreme velocities (Step C). When the trajectory breaches the separatrix into the unstable regime ($\Pi_1 > 1$), non-linear accretion outpaces decay. Here, stochastic fluctuations (Π_3) trigger structural symmetry breaking, deterministically forcing the tensor field to branch into the anisotropic dendritic architecture (Step B) to maximize transport conductance.

4.4. Spatiotemporal Evolution of Microbial Resistance

A central factor in bacterial survival is their capacity to evolve while spreading through environments with spatially varying challenges. The Microbial Evolution and Growth Arena (MEGA) plate enables direct observation of how bacterial populations expand and adapt across a large antibiotic landscape [25]. We postulate that the global morphology of the bacterial expansion is governed by the tensor evolution equation derived herein, where the evolutionary trajectory is defined by the interaction of the morphogenic number Π_1, the structural diffusion number Π_2, and the stochastic intensity Π_3. Within this triad, the deterministic boundaries of spatial coherence and metabolic viability are set by Π_1 and Π_2. Conversely, the biological variance required to probe the antibiotic landscape is supplied by the mutational noise parameter, Π_3. To simulate this microbial evolution, Equation (3) abstracts the biological matrix into a continuous conductivity field representing bacterial fitness and density. The conductivity tensor K represents the local phenotypic fitness and population density of the bacterial colony. It quantifies the facility with which the biological flux permeates the nutrient-antibiotic manifold Ω. It physically correlates with the local motility (v_{swim}) and the carrying capacity of the agar medium. The flux vector, defined by Equation (1), represents the total biomass flux vector seeking to maximize metabolic intake. It comprises both the diffusive spreading and the directed chemotactic drift driven by nutrient gradients ($-\nabla\phi$). As established in Section 2, simulating the system using Equation (3) requires a continuous driving flux to sustain structural accretion. Therefore, the tensor evolution must be explicitly coupled with a secondary diffusion-reaction equation to calculate the local scalar potential, representing the available nutrient or chemoattractant field. As the bacteria consume the nutrient field, the resulting biomass flux vector drives chemotactic drift towards higher nutrient concentrations. This dynamically calculated

flux is then fed continuously into Equation (3) to update the biological structure for the subsequent time step.

To capture the qualitative dynamics of the MEGA-plate experiment without relying on absolute biological constants, a Python simulation was performed using representative parameters that map directly to the deterministic terms governing the boundary dynamics. The source term $\alpha(J \otimes J)$ drivers the structural organization along flux lines. In this context, α represents the mutational susceptibility or the supply of adaptive mutations. This term captures the Hebbian non-linearity where successful colonization of a spatial region reinforces the genetic lineage, increasing the local conductivity for subsequent generations. In this simulation, this non-linear flux-induced accretion is driven with an accretion coefficient set to $\alpha = 1.2$. Counteracting this is the dissipation term $-\beta K$, which represents the thermodynamic cost of survival in a hostile environment. Physically, β identifies with the antibiotic-induced mortality rate or the metabolic tax required to maintain resistance mechanisms. To reflect the discrete physical architecture of the MEGA-plate, this decay parameter cannot be modeled as a constant. It features a basal background death rate of $\beta_{basal} = 0.0$ but spikes to $\beta_{step} = 1.5$ at specific spatial boundaries to represent the 10-fold and 100-fold discrete jumps in antibiotic concentration. Finally, the diffusion term $\gamma\nabla^2 K$ accounts for the random motility and spatial regularization of the bacterial front, ensuring physical continuity of the colony and penalizing infinite population density gradients. This spatial smoothing term is set to $\gamma = 0.05$ to represent the random motility (D_{mot}) of the bacteria in the soft agar. Finally, random stochastic fluctuations scaled by an intensity of 0.01 are incorporated to represent the essential random de novo mutations. These microscopic seeds are critical to the physical accuracy of the model, as they provide the necessary perturbations that allow a mutant to break symmetry and penetrate the antibiotic barrier once the deterministic front initially stalls.

To map these biological concepts to a stability diagram, we consider the nondimensionalization of Equations (3) and (4), normalizing against the characteristic scales of the experimental apparatus, the macroscopic domain length L (plate size), the nutrient driving force ϕ_0, and the reference motility K_0. This transformation, yielding the canonical evolution equation (Equation (6)), reveals that the evolutionary state of the system is defined by the morphogenic number Π_1, which represents the ratio of the mutational drive to the antibiotic resistance.

We identify two distinct physical regimes controlled by these parameters. The mutational drive parameter α scales with the population size N and mutation rate μ. In the context of the MEGA–plate, the power is determined by the mutational supply, which is a function of the wavefront area. Thus, the effective drive scales with the spatial extent of the front. In addition, the selection parameter β represents the ratio of antibiotic toxicity to intrinsic growth rates. In the experiment of Baym et al. [25], this is explicitly identified with the steepness of the antibiotic gradient steps (e.g., 10-fold vs. 100-fold increases).

The evolution of the system can be understood as a trajectory through the Π_1–Π_2 phase space governed by Equation (6) and can be simulated for the evolutionary phenomena observed empirically in the MEGA–plate experiment. Figure 2 presents a spatiotemporal simulation of microbial evolution and resistance on a varying antibiotic landscape using our coupled field-theoretic framework. The color map visualizes the continuous bacterial fitness and density field, evolving through the deterministic competition between flux-induced mutational accretion, spatial smoothing, and a spatially varying entropic decay. Consider the initial state of the inoculation at the edge of the MEGA–plate. The dominant driving force is the unidirectional nutrient gradient into the open agar, rendering the initial biomass flux J uniform and laminar. In this regime, the tensor is isotropic along the propagation axis, predicting a runaway expansion characterizing standard Fisher–KPP wave dynamics.

As shown in the simulation sequence, the bacterial front begins with a uniform, laminar expansion through the drug-free zone (β_{basal} = 0.0). However, this uniform solution abruptly stalls at the first boundary (indicated by the red dashed line) as the system encounters a discrete spike in antibiotic concentration (β_{step} = 1.5). The conservation of mass imposes a toxicity barrier that acts as a near-infinite resistance to the wild-type phenotype, manifesting as a divergence in the decay coefficient β. This localized spike in entropic decay completely overwhelms the mutational drive, plunging the morphogenic number below the critical threshold of unity ($\Pi_1 < 1$). The linear dissipation term $-\beta K$ overwhelms the growth term $\alpha(J \otimes J)$, forcing the macroscopic front to stagnate into a stalled, isotropic state. Because the system can no longer process the inflow efficiently through an isotropic geometry, the configuration must evolve to find a path of lower resistance, necessitating a morphological bifurcation. The resulting simulation panel demonstrates the colony stalling into a dead state, precisely mirroring the high step experiments empirically captured in Figure 2A of the Baym et al. [25] study, where extremely steep gradient jumps halt uniform progression entirely.

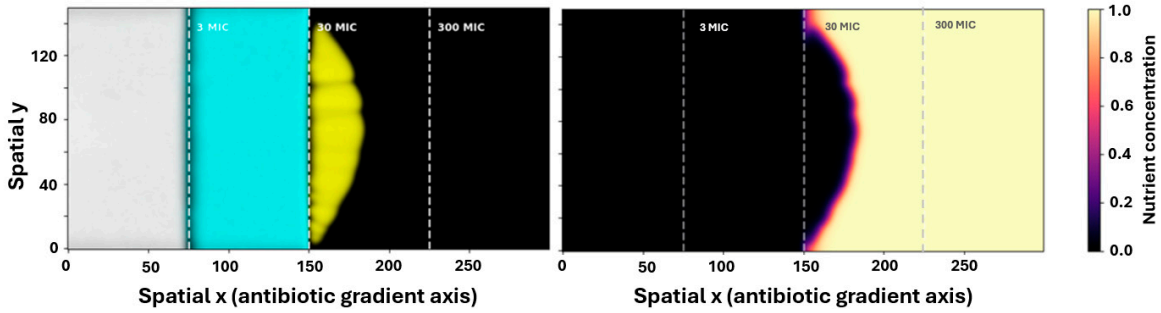

Figure 2. Field-theoretic simulation of microbial evolution on an antibiotic gradient plate. The left panel tracks the spatial distribution of four distinct bacterial lineages—Wild Type (grey) and successive Mutants 1–3 (cyan, yellow, and black, respectively)—propagating across increasing antibiotic thresholds (3, 30, and 300 MIC). The simulation accurately reproduces the macroscopic stalling of the Wild Type front (where antibiotic toxicity forces $\Pi_1 < 1$) and the subsequent symmetry-breaking and "sectoral fanning" (where stochastic mutations Π_3 allow the system to locally recover $\Pi_1 > 1$), directly mirroring the empirical time-lapse data in Figure 1C of Baym et al. [25]. The right panel depicts the corresponding depletion of the scalar nutrient field. This thermodynamic screening physically derives the "trapped mutant" phenomenon (observed in Figure 4 of Baym et al. [25]): highly conductive primary branches rapidly consume the available nutrient flux, establishing a localized thermodynamic dominance that starves adjacent secondary branches. This dynamically drops the local available potential ϕ, preventing fully resistant mutants from advancing if they nucleate behind the primary front.

Escape from this evolutionary dead-end relies entirely on the noise floor defined by Π_3. While microscopic fluctuations in fitness are suppressed by deterministic growth during the initial laminar expansion, the stalled front becomes hypersensitive to mutational noise. From this stalled equilibrium, stochastic de novo mutational fluctuations (noise intensity = 0.01) provide the necessary microscopic seeds to trigger a localized Mullins–Sekerka instability. These random, microscopic loci (single mutants) possess a lower local β and are naturally amplified, breaking the uniform macroscopic symmetry. Rather than forming microscopic fractal fingers, bacterial motility smooths these breakthroughs into broad, advancing macroscopic lobes that fan out into the high-drug territory. This anisotropy splits the flux vector J into stalled parent sectors and expanding resistant fronts. This formation of a resistant lineage requires the accretion power (mutational supply) to overcome the dissipation density (drug toxicity), governed by the quantifiable threshold where the growth rate exceeds the decay rate ($\Pi_1 > 1$).

Mapping Π_1 to biological variables, we find the critical condition where the mutation rate times the population size exceeds the death rate caused by the drug step. The numerator (Equation (8)) represents the macroscopic realization of the accretion term, quantifying the system capacity to convert metabolic flux into structural adaptation. Specifically, for [25], the effective structuring coefficient α is physically instantiated by the product of the population size at the wavefront and the intrinsic mutation rate, which determines the probabilistic supply of resistant genotypes capable of exploiting the flux. This is coupled with the expansion velocity, representing the magnitude of the convective flux that drives the encounter rate with the new environment. The denominator represents the magnitude of the dissipation coefficient β. To satisfy the thermodynamic dimensions of a decay rate, we define $\beta = k_d \ln(\Delta C)$, where k_d is a basal mortality rate constant and $\ln(\Delta C)$ represents the steepness of the antibiotic gradient step. This logarithmic dependence reflects the thermodynamic nature of the barrier: a steeper gradient imposes a higher energetic penalty on the wild-type conductivity field, effectively increasing the damping rate that the morphogenic drive must overcome.

To ensure dimensional consistency when scaling the continuous tensor field to macroscopic biological observables, the effective accretion rate must scale with the rate at which the population traverses the characteristic length L of the drug step (v_{swim}/L). This is formalized by the specific dimensionless morphogenic number for the MEGA–plate system

$$\Pi_1 = \frac{\mu N_{front} v_{swim}}{L k_d \ln(\Delta C)}, \tag{14}$$

where N_{front} is the population size at the wavefront, v_{swim} is the expansion velocity, μ is the intrinsic mutation rate, L is the macroscopic length scale of the gradient step, and k_d is the basal mortality rate.

Notice that the morphogenic number Π_1 dictates the gain of the positive feedback loop. When the mutational potential exceeds the entropic barrier, the system satisfies $\Pi_1 > 1$, and the accretion term dominates the relaxation term, triggering the spontaneous symmetry breaking into dendritic fingers. Below this threshold (as seen in the high step experiments (Figure 2A of Baym et al. [25]), where the denominator $\ln(\Delta C)$ is large), the non-linear term is insufficient to sustain a self-organized channel, and the system decays to a homogeneous, dead state.

The evolution of the system is determined by the interaction of three groups. While Π_1 determines the stability of the growth, the spatial coherence and texture of the resulting bacterial branches are governed by Π_2. This parameter defines the intrinsic correlation length of the architecture relative to the macroscopic domain, representing the competition between the diffusive smoothing term ($\gamma = D_{mot}$) and the selective dissipation ($\beta = k_d \ln(\Delta C)$), defined by

$$\Pi_2 = \frac{D_{mot}}{L^2 k_d \ln(\Delta C)}, \tag{15}$$

In the microbial context, D_{mot} is the diffusion coefficient of the bacteria in soft agar. To complete this tri-parameter framework for the microbial system, we introduce the stochastic intensity number Π_3, which governs the ratio of random mutational fluctuations to the deterministic relaxation rate. In the context of antibiotic landscapes, it represents the variance of the mutational noise relative to the metabolic tax of the drug. It is written as

$$\Pi_3 = \frac{\sigma_\xi}{k_d \ln(\Delta C) K_0}, \tag{16}$$

Here, σ_ξ represents the characteristic intensity of de novo mutations (i.e., the random phenotypic variations that probe the environment) while the denominator reflects

the entropic barrier imposed by the antibiotic gradient. While it triggers the necessary symmetry breaking by promoting microscopic mutants, an excessive Π_3 can disrupt the global coherence of the network, leading to a fragmented morphology where deterministic ordering is partially overwhelmed.

In the MEGA–plate experiment, bacterial motility D_{mot} allows the population to expand cohesively. This moderate Π_2 suppresses the formation of infinitely sharp, microscopic dendrites, instead forcing the macroscopic symmetry breaking to manifest as broad, sweeping lobes and expanding sectors of resistant lineages. The system smooths out microscopic differences between adjacent mutants, resulting in macroscopic spatial domains of distinct genetic territories. As these primary resistant branches shoot forward, they induce a profound non-local screening effect governed by the coupled nutrient field. In the final developed stage, highly conductive primary branches aggressively propagate into the high-drug territory. By rapidly consuming the available nutrient flux, they establish a localized thermodynamic dominance that effectively starves adjacent, slower regions. This nutrient screening mechanism physically reproduces the counterintuitive "trapped mutant" phenomenon experimentally documented in Figure 4 of the Baym et al. [25] study, where even highly resistant mutants are suppressed behind the propagating front because they lack the chemoattractant potential required to advance. The ability of the model spatial screening mechanics to physically replicate the suppression of fully resistant mutants behind the primary front, as mapped in Figure 4 of the [25], validates the thermodynamic basis of microbial competition. Furthermore, this trapped mutant phenomenon arises when the screening from a high K primary branch suppresses the local flux J available to a secondary branch, effectively starving it of the nutrient potential ϕ required to propagate.

In summary, the intersection of these energetic thresholds defines the bifurcation topology of the system, illustrated in the phase diagram (Figure 3). The transition between the diffusive/extinction phase and the resistant jet phase is not an artifact of random variation alone, but the deterministic equilibrium solution of the tensor evolution equation triggered by the stochasticity of Π_3. Just as a physical fracture is the necessary mechanical solution to relieve stress in a solid barrier, the macroscopic, lobed sectoring of resistant bacterial lineages is the necessary spatial configuration for biological flux to traverse the antibiotic landscape, emerging precisely when the non-linear constructal drive overwhelms the thermodynamic constraints of the chemical gradient. Ultimately, this demonstrates that microbial range expansion is not just a genetic process, but a deterministic thermodynamic phenomenon constrained by flux facilitation and spatial competition.

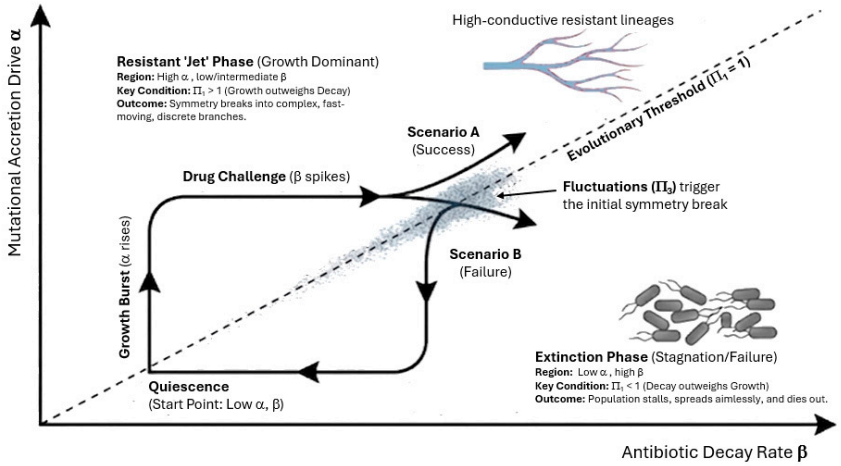

Figure 3. Constructal stability phase diagram of microbial resistance evolution. The macroscopic phase space is spanned by the flux-induced mutational accretion drive ($\alpha \propto \mu N_{front}\, v_{swim}$) and the resistive

thermodynamic cost of the antibiotic gradient ($\beta \propto k_d \ln(\Delta C)$). The dashed separatrix delineates the critical bifurcation threshold ($\Pi_1 = 1$). In the sub-critical Extinction Phase ($\Pi_1 < 1$), antibiotic toxicity overwhelms mutational supply, forcing the population to stall into an isotropic state. When the trajectory breaches the separatrix into the super-critical Resistant "Jet" Phase ($\Pi_1 > 1$), stochastic mutational noise (represented by the shaded Π_3 region) triggers localized symmetry breaking. Because bacterial motility maintains a finite structural diffusion number (Π_2), this symmetry breaking is physically smoothed into globally coherent macroscopic lobes (Scenario A) rather than microscopic fragmentation, allowing high-conductivity lineages to successfully penetrate the antibiotic barrier. Failure to sustain $\Pi_1 > 1$ results in a return to the stalled, isotropic state (Scenario B).

4.5. Morphological Phase Transitions in Black Hole Accretion and Relativistic Jets

The evolution of astrophysical structures, from protostellar clouds to the violent outflows of active galactic nuclei [26–28], has traditionally been modelled through complex magnetohydrodynamic force-balance equations. We postulate that the macroscopic morphology of the accretion flow, specifically the spectral state transitions and the launching of relativistic jets, is fundamentally governed by the tensor evolution equation derived herein. In this high-energy regime, the field variables in Equation (3) map directly to the components of the stress-energy tensor governing General Relativistic Magnetohydrodynamics. The conductivity tensor K represents the effective transport capacity of the accretion medium, quantifying the facility with which matter and angular momentum flow through the spacetime metric, correlating with the effective turbulent viscosity of the disc. The flux vector J constitutes the total energy-momentum flux. The source term $\alpha(J \otimes J)$ mathematically mirrors the anisotropic Maxwell stress tensor. In the disc, it drives the magneto-rotational instability, while near the event horizon, it represents the buildup of large-scale poloidal magnetic fields, the Magnetically Arrested Disc state, necessary for the Blandford–Znajek process [27]. This structural organization is counterbalanced by the dissipation term $-\beta K$, representing the thermodynamic cost of radiative cooling, while the diffusion term $\gamma \nabla^2 K$ accounts for the viscous spreading and structural coherence of the plasma.

To map the morphological transitions of the system, we evaluate the canonical dimensionless evolution equation (Equation (6)). The thermodynamic state of the black hole system is fully parametrized by the three dimensionless control parameters: the morphogenic number Π_1, the structural diffusion number Π_2, and the stochastic intensity Π_3. While Π_1 and Π_2 define the energetic drive and vertical coherence of the flow, the noise scaled by Π_3 represents the intrinsic MHD turbulence and stochastic fluctuations in the magnetic field topology that probe the stability of the accretion manifold. Here, the abstract accretion coefficient α scales with the square of the dimensionless black hole spin parameter (a^{*2}), while spatial smoothing is governed by the standard kinematic viscosity parameter (α_{visc}). For relativistic outflows, we define these parameters as

$$\Pi_1 = \frac{a^{*2}}{\lambda_{Edd}}, \Pi_2 = \frac{\alpha_{visc}(H/R)^2}{\lambda_{Edd}}, \Pi_3 = \frac{\sigma_B}{\lambda_{Edd}}, \tag{17}$$

where a^* is the dimensionless spin parameter of the black hole (representing the energetic drive of the central engine), and λ_{Edd} is the Eddington ratio (representing the efficiency of radiative cooling), α_{vis} is the standard viscosity parameter, σ_B represents the stochastic intensity of magnetic fluctuations or the variance of the Magnetohydrodynamic (MHD) turbulence, and H/R is the disk aspect ratio.

The topological transition between the standard disk state and the relativistic jet state (Figure 4) is a deterministic consequence of the interplay between these dimensionless parameters. The intersection of these thresholds defines the bifurcation point in the phase

diagram depicted in Figure 4. Through this, we can identify two distinct phenomenological regimes corresponding directly to observed X-ray spectral states, which are topologically distinguished by the structural diffusion number Π_2.

In regimes characterized by a high mass accretion rate, the disk is optically thick and cooling is highly efficient (λ_{Edd} is high). This massive radiative cooling acts as a severe thermodynamic penalty on the system, manifesting as a profoundly high dissipation coefficient β. Because λ_{Edd} is in the denominator of both control parameters, efficient cooling drives a simultaneous collapse of both Π_1 and Π_2. The collapse of the structural diffusion number ($\Pi_2 << 1$) means the smoothing force $\gamma\nabla^2 K$ is overpowered by the entropic decay $-\beta K$. Occupying this region of high thermodynamic cost (high β), the system lacks vertical coherence, and high radiative decay suppresses vertical growth, mathematically forcing the matter to collapse into a geometrically thin configuration (the Shakura–Sunyaev thin disk). Because the disk is geometrically thin, it cannot anchor the large-scale poloidal magnetic fields necessary for an outflow. Simultaneously, the collapse of the morphogenic number ($\Pi_1 < 1$) guarantees that radiative decay completely suppresses the non-linear magnetic accretion drive. Consequently, the system remains locked in a stable, structurally isotropic 2D sheet, and the relativistic jet is completely quenched.

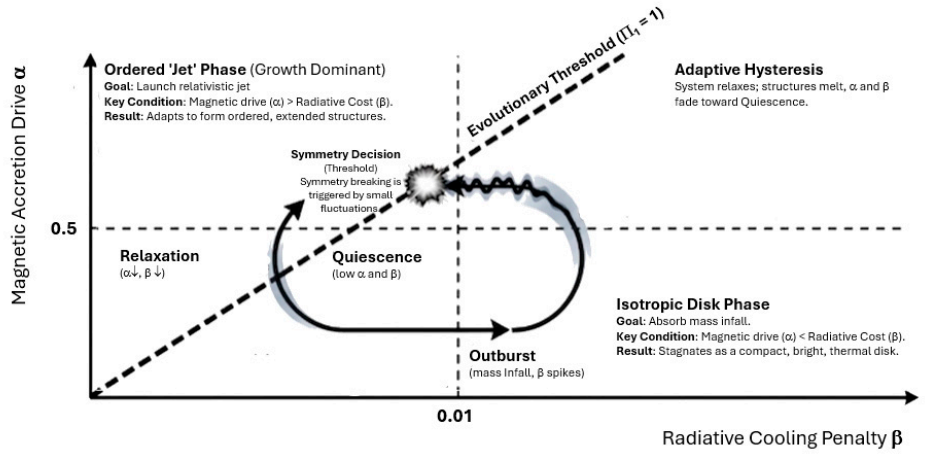

Figure 4. Constructal stability phase diagram of black hole accretion flows and jet launching. The macroscopic phase space is spanned by the flux-induced magnetic accretion drive ($\alpha \propto a^{*2}/\lambda_{\mathrm{Edd}}$) and the resistive thermodynamic penalty of radiative cooling ($\beta \propto \dot{m}$). The evolutionary trajectory deterministically mirrors the standard q-shaped hysteresis loop observed in the Hardness-Intensity Diagrams of X-ray binaries [26–28]. In the high-$\dot{m}$ Outburst Phase ($\Pi_1 < 1$), severe radiative decay (β) suppresses vertical growth, collapsing the structural diffusion number ($\Pi_2 << 1$) and forcing the system into a stable, geometrically thin isotropic disk. As the accretion rate drops, radiative cooling becomes inefficient (the ADAF regime, $\dot{m} \leq 0.01$), causing Π_2 to surge and the disk to expand into a geometrically thick torus. This macroscopic vertical coherence (Π_2) allows the trajectory to breach the critical separatrix ($\Pi_1 = 1$). This critical point marks the symmetry-breaking bifurcation where the system satisfies the dimensionless constructal criteria $a^* \geq 0.5$ and $\dot{m} \leq 0.01$. In this super-critical regime, stochastic MHD turbulence (represented by the Π_3 noise region) triggers symmetry breaking. The non-linear magnetic drive (α) overpowers decay, deterministically forcing the structural tensor to branch into a highly collimated relativistic jet to maximize energy flux.

As the mass supply drops, the system crosses a critical threshold where radiative cooling becomes vastly inefficient (the ADAF regime, characterized by low λ_{Edd}). This transition is constrained by the limits of advective solutions. The standard ADAF solution exists only for accretion rates $\dot{m} < \alpha_{visc}^2$. By adopting the standard Shakura–Sunyaev viscosity parameter $\alpha_{\mathrm{visc}} \sim 0.1$, the critical threshold emerges as $\dot{m}_{crit} \sim 0.01$. In this mapping, the dimensionless dissipation coefficient β represents the radiative cooling

efficiency. Because the radiative cooling rate scales as $\dot{m}^2$ while viscous heating scales as $\dot{m}$, the thermodynamic penalty of the system is directly proportional to the normalized accretion rate ($\beta \propto \dot{m}$). Thus, dropping below $\dot{m}_{crit}$ profoundly alters the thermodynamic stability of the field. As the cooling efficiency plummets, the dissipative penalty β collapses, triggering a triple-parameter phase transition. First, the macroscopic structural diffusion number Π_2 surges. The energetic penalty for maintaining structure diminishes, and the spatial smoothing term $\gamma\nabla^2 K$ dominates. This forces the accretion flow to expand vertically into a geometrically thick torus (H/R~1). This high Π_2 regime (low β, low luminosity) provides the macroscopic vertical structural coherence that enables the magnetic drive to dominate, allowing magnetic field lines to remain aligned over vast distances without breaking up into localized turbulence. This constraint ensures that if $\beta > 0.01$ (low Π_2), radiative decay suppresses coherent structures, but if $\beta < 0.01$ (high Π_2), the decay term vanishes and the anisotropic growth term takes over. Second, with the radiative decay term neutralized ($\beta < 0.01$), the non-linear magnetic accretion drive takes over. From the Blandford–Znajek mechanism, the jet power scales as ka^{*2} [29]. Mapping α to the spin parameter, we find the critical condition $a^{*2} \geq C_{vac}$, where C_{vac} is a vacuum coupling constant typically of about 0.25 [29], yielding a critical spin of 0.5.

If the black hole possesses sufficient spin ($a^* \geq 0.5$), the system effortlessly breaches the critical morphogenic threshold ($\Pi_1 > 1$), though the actual transition remains dormant until nucleated. Finally, the dormant symmetry breaking is ignited by the stochastic fluctuations represented by Π_3. While the global torus provides the reservoir of energy and structural coherence, the noise floor of Π_3 provides the initial magnetic perturbations required to escape the quasi-isotropic ADAF state and establish the poloidal flux alignment. The specific geometry of this symmetry breaking is a strict mathematical consequence of the interaction between these three parameters. In the equatorial plane, the high density of the thick ADAF torus maintains a finite structural diffusion number (Π_2), which regularizes the flow and manages the viscous inflow. However, along the centrifugal barrier of the polar axis, matter density plummets. Consequently, the matter-dependent smoothing term ($\gamma\nabla^2 K$) functionally vanishes in the polar funnel. Relieved of this spatial constraint, the dyadic tensor interaction $\alpha(J \otimes J)$, which in this regime mathematically mirrors the anisotropic Maxwell stress tensor of a Magnetically Arrested Disk, experiences a runaway non-linear feedback loop. The local magnetic energy density overwhelms the rest-mass energy density, creating a massive geometric divergence that mathematically forces the structure to elongate into a highly collimated relativistic jet. Thus, the launch of a relativistic jet is not an artifact of random magnetic alignment, but the inevitable, deterministic equilibrium state of a rotating, self-gravitating flow system where the stochastic seeds of Π_3 are amplified by the non-linear constructal drive of Π_1.

5. Conclusions

This study has established a general field-theoretic formalism for the evolution of flow architectures, elevating the domain configuration from a static boundary condition to a conductivity tensor field K that co-evolves with the currents it supports. By postulating a canonical evolution equation governed by the competition between non-linear accretion $\alpha(J \otimes J)$, entropic dissipation $-\beta K$, and structural diffusion $\gamma\nabla^2 K$, we have derived the emergence of global flow architecture as a deterministic solution to local thermodynamic constraints. Central to this framework is the identification of morphology as a thermodynamic state. The transition from isotropic, diffusive structures, such as spheres, mounds, or stalled fronts, to anisotropic, convective structures like dendrites and jets is formally identified as a symmetry-breaking phase transition.

This bifurcation is controlled by a dimensionless morphogenic number Π_1, which acts as the primary control parameter of the system. Complementing this, the structural diffusion number Π_2 governs the complexity density of the evolved architecture, determining whether the system manifests as fine-grained fractal networks or globally coherent conduits. The stochastic intensity Π_3 completes this tri-parameter framework by defining the threshold of structural stability and providing the essential microscopic perturbations required to trigger symmetry breaking. While Π_1 and Π_2 define the energetic and structural landscape of the manifold, Π_3 acts as the causal agent that allows the system to escape unstable isotropic states. As explicitly derived for the aerosol and biophysical systems, Π_2 is not a static background parameter. It collapses dynamically as the system's characteristic screening length (such as the aggregate dimension D or the diffusion depletion layer L_{disp}) expands. We demonstrated that whenever the flow-induced drive exceeds the entropic decay ($\Pi_1 > 1$) in conjunction with this rapid drop in spatial regularization, the system inevitably undergoes a localized symmetry-breaking bifurcation. By integrating Π_3 into the canonical evolution, we have demonstrated that the "path of least resistance" is not merely a static geometric optimum but a dynamic equilibrium reached through the amplification of stochastic seeds. The system must then spontaneously instigate high-conductivity geometries, scaled precisely by Π_2 and seeded by the fluctuations of Π_3, to satisfy the second law of thermodynamics. This confirms that the emergence of design is a process of exploration and settlement, where stochastic noise is harvested by the non-linear constructal drive to reach the most efficient transport state.

Despite its trans-scalar applicability, this field-theoretic approach possesses inherent limitations regarding its spatial-temporal scales and degrees of freedom. By treating the conductivity tensor K as a continuous macroscopic variable, the framework relies on a continuum approximation. It acts effectively as a coarse-grained model, assuming the structural medium contains sufficient microscopic degrees of freedom to be statistically averaged. Consequently, this continuous formulation will break down at the extreme microscopic limits (such as single-molecule transport or quantum tunneling regimes) where discrete, individual particle interactions dominate and the statistical validity of a continuous tensor field dissolves.

The broad applicability of this description is underscored by the successful application of the single tensor equation to systems spanning several orders of magnitude, ranging from the electrostatic aggregation of aerosol particles and the hydrodynamics of stony corals to the evolutionary dynamics of microbial resistance and the relativistic outflows of active galactic nuclei. This suggests that these diverse phenomena belong to the same general class, wherein design is not an artifact of specific material properties but a general geometric response to the imperative of flux facilitation. Furthermore, this formalism provides a mathematical derivation of the constructal principle, demonstrating that the principle of "easier access" is not a goal-oriented axiom but an asymptotic result of field evolution. The tensor interaction ensures that the system actively minimizes its own resistance over time, identifying the "path of least resistance" through a continuous process of stress-induced adaptation. Finally, this study suggests that flow architecture, whether the branching of a bacterial lineage or the collimation of an astrophysical jet, is the inevitable stationary state equilibrium of nonequilibrium matter. Just as the sphere is the necessary shape for minimizing surface energy, the dendrite is the necessary shape for maximizing flux, emerging precisely when the non-linear constructal drive overwhelms the thermodynamic constraints of the diffusive regime.

Funding: The author gratefully acknowledges the financial support provided to the Institute of Earth Sciences through the multi-annual funding agreement with the Foundation for Science and Technology of Portugal (FCT), under project UID/04683.

Data Availability Statement: The data that support this study are available from the author upon reasonable request.

Conflicts of Interest: The author declares no conflicts of interest.

Nomenclature

Latin Symbols

C_0	Global resource pool constraint (varies by regime)
D	Characteristic microscopic dimension [L]
J	Generalized flux density vector (varies by regime)
K	Configuration/Conductivity second-rank tensor (varies by regime)
K_0	Reference conductivity imposed by global resource constraint (varies by regime)
L	Macroscopic domain size/characteristic length scale [L]
L_{disp}	Macroscopic diffusion boundary layer [L]
r_0	Intrinsic structural length scale [L]
t	Time [T]
u	Local material velocity field [L][T]$^{-1}$

Greek Symbols

α	Structuring/flux-induced accretion coefficient (varies by regime)
β	Entropic dissipation/linear decay coefficient [T]$^{-1}$
γ	Structural diffusion/spatial smoothing coefficient [L]^2[T]$^{-1}$
ϕ	Scalar potential/intensive driving force (varies by regime)
σ	Local dissipation density (varies by regime)
τ	Characteristic relaxation time of the structural medium
ξ	Stochastic field/white noise (varies by regime)

Dimensionless Groups and Normalized Variables

Π_1	Morphogenic number (ratio of accretion drive to entropic decay)
Π_2	Structural diffusion number (ratio of spatial cohesion to decay)
Π_3	Stochastic intensity number (ratio of noise to relaxation rate)
a^*	Dimensionless black hole spin parameter
$\dot{m}$	Normalized mass accretion rate (Eddington ratio)
K*	Dimensionless conductivity tensor
J*	Dimensionless generalized flux density
ϕ*	Dimensionless scalar potential
t*	Dimensionless time
x*	Dimensionless spatial coordinate

Appendix A

To establish a foundation for the dynamic evolution of flow architectures, we can derive the governing tensor equation from first principles using a variational approach based on non-equilibrium thermodynamics. Our model relies on the following assumptions: (i) the system is strictly gradient-driven; (ii) the structural matrix is a yielding medium capable of dynamic reconfiguration; and (iii) the free energy can be expanded following lowest-order permitted symmetries (Ginzburg–Landau approach [17]).

We begin by defining the state of the system through the configuration field K(x, t), which is defined as a symmetric second-rank tensor representing the local constitutive properties of the manifold. In the framework of linear irreversible thermodynamics, a system driven far from equilibrium will continuously evolve its internal state variables to minimize a generalized free energy or, equivalently, maximize its rate of entropy production constrained by internal dissipation. We consider the existence of a scalar functional F[K], which integrates the local thermodynamic costs and driving forces over the generalized n-dimensional manifold Ω. This functional is constructed from the lowest-order scalar

invariants permitted by the spatial symmetries of the tensor K(x, t) and the local flux vector J(x, t). The functional F[K] accounts for three distinct physical tendencies: positive feedback, entropic relaxation, and spatial regularization. First, the thermodynamic drive to facilitate flow acts to align the principal axes of the conductivity tensor with the prevailing flux. The simplest scalar invariant that couples the flux vector to the conductivity tensor while preserving transmission symmetry is the contraction of K the dyadic product $J \otimes J$. We assign this a coupling constant α, the structuring coefficient. Second, maintaining structural order away from an isotropic background state incurs an energetic penalty. The lowest-order positive-definite scalar invariant representing this entropic cost is proportional to the trace of the square of the tensor, scaled by a dissipation coefficient β. Notice that, while β acts locally as a thermodynamic penalty for structural ordering, it concurrently functions as a dynamic Lagrange multiplier when evaluating the system macroscopically. By dynamically adjusting this coefficient, the system enforces a global resource constraint, ensuring that the total structural volume (or conductance) is conserved across the domain during morphological evolution. Finally, the physical medium possesses an intrinsic structural stiffness or surface tension that penalizes abrupt spatial variations. This spatial regularization is captured by the square of the tensor gradient, scaled by a diffusive coefficient γ. Following the Ginzburg–Landau approach [17] of expanding the free energy to the lowest-order permitted symmetries, the total functional takes the form

$$F[\mathrm{K}] = \int_{\Omega} \left[-\alpha Tr((J \otimes J).\mathrm{K}) + \frac{\beta}{2} Tr\mathrm{K}^2 + \frac{\gamma}{2} |\nabla K|^2 \right] d^n x, \tag{A1}$$

To explicitly define the link between the Ginzburg–Landau functional and the underlying thermodynamic fluxes, it is important to note that F[K] serves as a generalized thermodynamic potential (or Lyapunov functional) for the structural manifold. Rather than being a heuristic 'inspiration,' the functional is constructed by expanding the free energy to the lowest-order permitted tensor symmetries, where the non-linear coupling term $\alpha Tr((J \otimes J).\mathrm{K})$ represents the work done by the flux vector in ordering the conductivity field. This formulation ensures that the local relaxation of the tensor K follows a deterministic path of constrained entropy production, mapping the abstract variational descent directly to the physical maximization of flow access. By utilizing this framework, the emergence of architecture is established as a formal boundary-value problem where the physical constants (α, β, γ) are determined by the constitutive properties of the medium rather than arbitrary fitting.

In component notation, utilizing the Einstein summation convention, the integrand density ϑ is written as

$$\vartheta = -\alpha J_i J_j \mathrm{K}_{ij} + \frac{\beta}{2} \mathrm{K}_{ij} \mathrm{K}_{ij} + \frac{\gamma}{2} \left(\partial_k \mathrm{K}_{ij} \right) \left(\partial_k \mathrm{K}_{ij} \right), \tag{A2}$$

To determine the dynamic evolution of the configuration field, we apply model A of the Hohenberg–Halperin classification for relaxational dynamics [30]. This principle dictates that the order parameter K(x, t) evolves strictly downhill in the energy landscape, seeking to locally minimize the functional F at a rate inversely proportional to a characteristic relaxation time τ. The governing equation is defined by the negative of the functional derivative

$$\tau \frac{\partial \mathrm{K}_{ij}}{\partial t} = -\frac{\delta F}{\delta \mathrm{K}_{ij}}, \tag{A3}$$

To evaluate the functional derivative $\frac{\delta F}{\delta K_{ij}}$, we apply the standard Euler–Lagrange operator to the integrand density ϑ

$$\frac{\delta F}{\delta K_{ij}} = \frac{\partial \vartheta}{\partial K_{ij}} - \partial_k \left[\frac{\partial \vartheta}{\partial (\partial_k K_{ij})} \right], \tag{A4}$$

Before evaluating the functional derivatives, it is necessary to address the implicit dependence of the flux vector J on the configuration tensor K, as given by the constitutive relation $J = -K.\nabla\phi$. A direct variation in the flux-coupling term $-\alpha J_m J_n K_{mn}$ would inherently require expanding the derivative of the flux. To resolve this, we invoke a strict separation of timescales via an adiabatic (or Born–Oppenheimer-like) approximation [31], formally executing the adiabatic elimination of fast-relaxing transport variables [32]. We consider that the characteristic relaxation time of the transport dynamics (t_{flow}) is infinitesimally small compared to the structural relaxation time (τ), $t_{flow} << \tau$. Under this thermodynamic constraint, the convective or diffusive flow adjusts instantaneously to the evolving geometry. Consequently, during the infinitesimal variational step δK, the system evolves in a landscape where the flux J acts as an adiabatically subjected, momentarily fixed driving field. Its variation with respect to the structural tensor is therefore negligible $\partial J_m / \partial K_{ij} \approx 0$. While a global variation would require explicit coupling of J and K through the continuity equation $\nabla . J = 0$ using a dynamically adjusting Lagrange multiplier field, the great timescale separation permits a local approximation via the principle of constrained entropy production. Because $t_{flow} << \tau$, the scalar potential field $\phi(x, t)$ instantaneously equilibrates across the domain Ω to enforce global mass conservation following any local perturbation in conductivity. Consequently, during the infinitesimal structural update δK, the local thermodynamic force $\nabla\phi$ can be treated as momentarily constant. Under this constraint of a fixed local driving force, the functional derivative acts strictly on the explicit geometry of the manifold, effectively decoupling the global kinematic constraints from the local thermodynamic descent. Thus, J is treated as an independent external field during the variation. Physically, this adiabatic decoupling is rigorous because in far-from-equilibrium open systems, the flux J embodies the convective kinetic energy of the flow. By treating J as a momentarily independent driving field, the non-linear term $\alpha(J \otimes J)$ mathematically functions as an injected momentum stress tensor (strictly analogous to the Reynolds stress in fluid turbulence or the Maxwell stress in magnetohydrodynamics) doing thermodynamic work to locally order the material matrix.

We can now evaluate the local derivatives of Equation (A4) term by term. The derivative of the flux-coupling term with respect to K_{ij} yields $-\alpha J_i J_j$. The derivative of the entropic relaxation term $\frac{\beta}{2} K_{mn} K_{mn}$ with respect to K_{ij} yields βK_{ij}. In evaluating the spatial regularization term, taking the derivative of the density with respect to the gradient $\partial_l K_{ij}$ yields $\gamma \partial_l K_{ij}$. Upon integrating by parts over the domain Ω and assuming the variations $\partial_l K_{ij}$ vanish at the boundaries, the divergence operator ∂_l is transferred to the field, resulting in the restorative diffusive force $\gamma \nabla^2 K_{ij}$.

Assuming the variations δK_{ij} vanish at the boundaries of the domain Ω, the total functional derivative evaluates to

$$\frac{\delta F}{\delta K_{ij}} = -\alpha J_i J_j + \beta K_{ij} - \gamma \nabla^2 K_{ij}, \tag{A5}$$

Substituting this result back into the relaxational dynamics equation yields the component-form evolution equation

$$\tau \frac{\partial K_{ij}}{\partial t} = \alpha J_i J_j - \beta K_{ij} + \gamma \nabla^2 K_{ij}, \tag{A6}$$

While Equation (A6) describes the local relaxational response, a comprehensive flow architecture model must satisfy the principle of objectivity within a medium undergoing macroscopic drift U(x, t). The current formulation utilizing the partial temporal derivative assumes a static coordinate frame, which is insufficient for systems where the structural field is advected by the underlying flow.

To resolve this, the partial derivative must be generalized to an objective tensor derivative, such as the corotational (Jaumann) rate or upper-convected Maxwell rate [33]. Specifically, the former is sufficient for rotation-dominated regimes where structural deformation is negligible, whereas the latter is strictly required in shear-dominated flows to accurately capture the physical stretching and continuous deformation of the tensor manifold. Unlike a scalar field, where the standard material derivative suffices, evaluating a second-rank tensor within a moving medium requires an objective rate to strictly account for fluid vorticity and strain, ensuring that the internal tensor axes physically rotate alongside the fluid elements. This ensures that the anisotropy and magnitude of the evolving conductivity are preserved along material characteristic trajectories rather than being pinned to a fixed spatial location. By accounting for the advection of order by the background flow, the model effectively couples the thermodynamic relaxation of the manifold to the kinematic transport of the medium.

Within this Model A relaxational framework, the order parameter K(x, t) evolves strictly downhill to locally minimize the energy functional F. However, the deterministic descent derived in Equation (A6) is fundamentally insufficient to capture the spontaneous symmetry breaking observed in driven media. From a perfectly isotropic initial state (K = 0), the system lacks the necessary perturbation to trigger structural alignment. To overcome this, we extend the relaxational dynamics by including a Langevin term ξ(x, t), representing the Gaussian white noise inherent to the medium. These stochastic fluctuations provide the physical catalyst, or seeds, required for the manifold to escape the unstable isotropic state and nucleate ordered architectures.

Transitioning the derivation back into absolute tensor notation, we must synthesize these requirements while strictly respecting the intrinsic symmetries of the underlying manifold. Because the flux J is a vector, its dyadic product $J \otimes J$ inherently produces a perfectly symmetric tensor. Consequently, the functional derivative of the scalar invariant yields the active generation term $\alpha(J \otimes J)$ natively, without any risk of generating non-physical anti-symmetric components. This mathematically guarantees that the active torque naturally evolves within the symmetric manifold of the configuration field K, rendering ad hoc phenomenological projections entirely unnecessary. Integrating this thermodynamic derivative with the requisite objective tensor rate and stochastic fluctuations, we arrive at the complete, frame-invariant evolution equation

$$\tau \overset{o}{K} = \alpha(J \otimes J) - \beta \mathrm{K} + \gamma \nabla^2 K + \xi(x, t) \tag{A7}$$

Here $\overset{o}{K}$ denotes the chosen objective rate. Rather than a purely conservative process, Equation (A7) represents the stochastic consequence of dissipative relaxational dynamics. While the deterministic terms describe the system descent through the energy landscape defined by the functional F, the Langevin framework provides the necessary mechanism for the manifold to escape unstable configurations and drive the flow architectures governed by the flux-coupling torque. This completes the self-organized feedback loop between the manifold geometry and the driving flux.

https://doi.org/10.3390/sym18050732

References

1. Bejan, A. *Shape and Structure, from Engineering to Nature*; Cambridge University Press: Cambridge, UK, 2000.
2. Bendsøe, M.P.; Sigmund, O. *Topology Optimization: Theory, Methods, and Applications*; Springer: Berlin/Heidelberg, Germany, 2003.
3. Prigogine, I. *Introduction to Thermodynamics of Irreversible Processes*; John Wiley & Sons: New York, NY, USA, 1967.
4. Martyushev, L.M.; Seleznev, V.D. Maximum entropy production principle in physics, chemistry and biology. *Phys. Rep.* **2006**, *426*, 1–45. [CrossRef]
5. Kadic, M.; Milton, G.W.; van Hecke, M.; Wegener, B. 3D metamaterials. *Nat. Rev. Phys.* **2019**, *1*, 198–210. [CrossRef]
6. Zheludev, N.I.; Kivshar, Y.S. From metamaterials to metadevices. *Nat. Mater.* **2012**, *11*, 917–924. [CrossRef] [PubMed]
7. Sigmund, O.; Maute, K. Topology Optimization Approaches—A Comparative Review. *Struct. Multidiscip. Optim.* **2013**, *48*, 1031–1055. [CrossRef]
8. Tang, T.; Wang, L.; Zhu, M.; Zhang, H.; Dong, J.; Yue, W.; Xia, H. Topology Optimization: A Review for Structural Designs Under Statics Problems. *Materials* **2024**, *17*, 5970. [CrossRef]
9. Bejan, A.; Lorente, S. The constructal law and the evolution of design in nature. *Phys. Life Rev.* **2011**, *8*, 209–240. [CrossRef]
10. Bejan, A.; Lorente, S. Constructal law of design and evolution: Physics, biology, technology, and society. *J. Appl. Phys.* **2013**, *113*, 151301. [CrossRef]
11. Bejan, A. The principle underlying all evolution, biological, geophysical, social and technological. *Philos. Trans. A Math. Phys. Eng. Sci.* **2023**, *381*, 20220288. [CrossRef]
12. Rodriguez-Iturbe, I.; Rinaldo, A. *Fractal River Basins: Chance and Self-Organization*; Cambridge University Press: Cambridge, UK, 1997.
13. West, G.B.; Brown, J.H.; Enquist, B.J. A general model for the origin of allometric scaling laws in biology. *Science* **1997**, *276*, 122–126. [CrossRef]
14. Niemeyer, L.; Pietronero, L.; Wiesmann, H.J. Fractal Dimension of Dielectric Breakdown. *Phys. Rev. Lett.* **1984**, *52*, 1033–1036. [CrossRef]
15. Maxwell, J.C. On Faraday's lines of force. *Trans. Camb. Philos. Soc.* **1858**, *10*, 27–83.
16. Einstein, A. Die Feldgleichungen der Gravitation. *Sitzungsber. K. Preuss. Akad. Wiss.* **1915**, *48*, 844–847.
17. Ginzburg, V.L. Some remarks on phase transitions of the second kind and the microscopic theory of ferroelectric materials. *Fiz. Tverd. Tela* **1960**, *2*, 2031–2043.
18. Reis, A.H.; Miguel, A.F.; Bejan, A. Constructal theory of particle agglomeration and design of air-cleaning devices. *J. Phys. D Appl. Phys.* **2006**, *39*, 2311–2318. [CrossRef]
19. Miguel, A.F. Constructal pattern formation in stony corals, bacterial colonies and plant roots under different hydrodynamics conditions. *J. Theor. Biol.* **2006**, *242*, 954–961. [CrossRef] [PubMed]
20. Miguel, A.F.; Bejan, A. The principle that generates dissimilar patterns inside aggregates of organisms. *Phys. A* **2009**, *388*, 727–731. [CrossRef]
21. Kaandorp, J.A.; Sloot, P.M.A. Morphological models of radiate accretive growth and the influence of hydrodynamics. *J. Theor. Biol.* **2001**, *209*, 257–274. [CrossRef] [PubMed]
22. Sekerka, R.F. Theory of crystal growth morphology. In *Crystal Growth—From Fundamentals to Technology*; Muller, G., Métois, J.-J., Rudolph, P., Eds.; Elsevier: Amsterdam, The Netherlands, 2004.
23. Mullins, W.W.; Sekerka, R.F. Morphological stability of a particle growing by diffusion or heat flow. *J. Appl. Phys.* **1963**, *34*, 323–329. [CrossRef]
24. Langer, J.S. Instabilities and pattern formation in crystal growth. *Rev. Mod. Phys.* **1980**, *52*, 1–28. [CrossRef]
25. Baym, M.; Lieberman, T.D.; Kelsic, E.D.; Chait, R.; Gross, R.; Yelin, I.; Kishony, R. Spatiotemporal microbial evolution on antibiotic landscapes. *Science* **2016**, *353*, 1147–1151. [CrossRef]
26. Ray, T.P.; Ferreira, J. Jets from young stars. *New Astron. Rev.* **2021**, *93*, 101615. [CrossRef]
27. Blandford, R.; Meier, D.; Readhead, A. Relativistic jets from active galactic nuclei. *Annu. Rev. Astron. Astrophys.* **2019**, *57*, 467–509. [CrossRef]
28. Frank, J.; King, A.; Raine, D.J. *Accretion Power in Astrophysics*; Cambridge University Press: Cambridge, UK, 2002.
29. Blandford, R.D.; Znajek, R.L. Electromagnetic extraction of energy from Kerr black holes. *Mon. Not. R. Astron. Soc.* **1977**, *179*, 433–456. [CrossRef]
30. Hohenberg, P.C.; Halperin, B.I. Theory of dynamic critical phenomena. *Rev. Mod. Phys.* **1977**, *49*, 435–479. [CrossRef]
31. Born, M.; Oppenheimer, R. Zur Quantentheorie der Molekeln. *Ann. Phys.* **1927**, *389*, 457–484. [CrossRef]

32. Haken, H. *Synergetics: An Introduction. Nonequilibrium Phase Transitions and Self-Organization in Physics, Chemistry, and Biology*; Springer: Berlin/Heidelberg, Germany, 1977.
33. Bird, R.B.; Armstrong, R.C.; Hassager, O. *Dynamics of Polymeric Liquids, Volume 1: Fluid Mechanics*; Wiley-Interscience: New York, NY, USA, 1987.